STUDIES OF SILICON PN JUNCTION SOLAR CELLS

By

Fredrik A. Lindholm, Principal Investigator
Department of Electrical Engineering
University of Florida
Gainesville, Florida 32611

FINAL TECHNICAL REPORT
covering the period July 24, 1975 - July 23, 1976

prepared for

National Aeronautics and Space Administration
NASA Lewis Research Center
NASA grant NSG-3018

STUDIES OF SILICON PN JUNCTION SOLAR CELLS

By

Fredrik A. Lindholm, Principal Investigator
Department of Electrical Engineering
University of Florida
Gainesville, Florida 32611

FINAL TECHNICAL REPORT
covering the period July 24, 1975 - July 23, 1976

prepared for

National Aeronautics and Space Administration
NASA Lewis Research Center
NASA grant NSG-3018

TABLE OF CONTENTS

FOREWORD

This report summarizes the major technical findings made in the research program at the University of Florida sponsored by NASA Lewis Research Center under Grant No. NSG-3018. This grant is a continuation of the support began under the same grant number on June 24, 1974. We report here our findings during the period of the grant: July 24, 1975 to July 24, 1976.

The work to be reported came from the efforts of several key people. C. T. Sah suggested to NASA the possibility of placing this grant research at the University of Florida, and afterwards, together with the author, helped make the arrangements and formulate the technical plan of the research. Dr. Sah has contributed significantly to nearly every aspect of the research described in this report. After joining the faculty of the University of Florida in September, 1976, Arnost Neugroschel became a key contributor to the research program. The technical collaboration of M. P. Godlewski and H. W. Brandhorst, Jr., of NASA Lewis Research Center greatly aided the completion of several phases of the research. During the tenure of the NASA grant, the Energy Research and Development Administration began supporting a separate but related research program at the University of Florida under the author's direction. This support aided the research reported here, and made possible a valuable and continuing technical interaction with J. G. Fossum of Sandia Laboratories (ERDA), Albuquerque, New

Mexico. E. L. Burgess of Sandia Laboratories also contributed to the research findings that we report. In addition to these senior investigators, several graduate students at the University of Florida participated in the research. They are: P. J. Chen, S. C. Pao, G. Badeaux, M. P. Callaway, and F. Therez.

Our research sponsored by NASA during the year (July 1975 to July 1976) produced the following technical papers:

1. F. A. Lindholm and C. T. Sah, "Process-Induced Defects in Terrestrial Solar Cells," Proceedings of the First ERDA Semiannual Solar Conversion Program Conference, Los Angeles, pp. 578-590, July 1975 (invited paper).

2. M. P. Godlewski, H. W. Brandhorst, Jr., F. A. Lindholm and C. T. Sah, "Experimental Investigation of the Diffused Layer of a 0.1 ohm-cm Silicon Solar Cell," Symposia of the 1976 Device Research Conference and the 1976 Electronic Materials Conference, Salt Lake City, Utah, June 23, 1976.

3. F. A. Lindholm and C. T. Sah, "Studies of Basic Mechanisms Influencing Solar Cell Efficiency for Terrestrial Applications," Proc. National Solar Photovoltaic Program Review Meeting, session III, paper 7, Orono, ME, 1976.

4. F. A. Lindholm, A. Neugroschel, and C. T. Sah, "Basic Mechanisms Governing Solar-Cells Efficiency," Proc. Int. Solar Energy Society, Vol. 6, pp. 120-129, Winnipeg, Manitoba, Canada, Aug. 1976.

5. F. A. Lindholm and C. T. Sah, "Normal Modes of pn Junction Devices for Material-Parameter Determination," J. Appl. Phys., Vol. 47, pp. 4203-4205, Sep. 1976.

6. F. A. Lindholm, C. T. Sah, A. Neugroschel, M. P. Godlewski, and H. W. Brandhorst, "Methodology for Experimental Determination of Gap Shrinkage and Lifetimes in Emitter and Base of pn Junction Solar Cells," Record of Twelfth Photovoltaic Specialists Conf., paper 1.1, Nov. 1976.

7. F. A. Lindholm, J. G. Fossum, and E. L. Burgess, "Basic Corrections to Solar Cell Performance Required by Inapplicability of Superposition," Record of Twelfth Photovoltaic Specialists Conf., paper 1.6, Nov. 1976.

8. F. A. Lindholm, A. Neugroschel, and C. T. Sah, "Junction Modeling for Solar Cells--Theory and Experiment," Tech. Digest 1976 Int. Electron Devices Meeting, 76CH1151-OED, pp. 61-65, Dec. 1976 (invited paper).

9. F. A. Lindholm, C. T. Sah, and J. G. Fossum, "Fundamental Considerations for Improving the Efficiency of Junction Silicon Solar Cells," Proc. National Solar Photovoltaic Program Review Meeting, session III, paper 1, San Diego, Calif., Jan. 1977.

10. F. A. Lindholm and C. T. Sah, "Fundamental Electronic Mechanisms Limiting the Performance of Solar Cells," IEEE Trans. Electron Devices, April 1977.

11. C. T. Sah and F. A. Lindholm, "Carrier Generation, Recombination, Trapping and Transport in Semiconductors with Position-Dependent Composition," IEEE Trans. Electron Devices, April 1977.

12. J. G. Fossum and F. A. Lindholm, "The Dependence of Open-Circuit Voltage on Illumination Level in p-n-Junction Solar Cells," IEEE Trans. on Electron Devices, April 1977.

13. F. A. Lindholm, A. Neugroschel, C. T. Sah, M. P. Godlewski, and H. W. Brandhorst, Jr., "Methodology for the Experimental Determination of Gap Shrinkage and Lifetimes in the Emitter and Base of p-n Junction Solar Cells and Other p-n Junction Devices," IEEE Trans. Electron Devices, April 1977.

14. A. Neugroschel, F. A. Lindholm, and C. T. Sah, "A Method for Determining the Emitter and Base Lifetimes in p-n Junction Diodes," IEEE Trans. Electron Devices, June 1977.

15. M. P. Godlewski, H. W. Brandhorst, Jr., F. A. Lindholm, and C. T. Sah, "Experimental Investigation of Excess Charge and Time Constant of Minority Carriers in the Diffused Layer of 0.1 ohm-cm Silicon Solar Cell," Int. J. Electronic Materials, accepted for publication.

In addition, the author gave seminars on results of our NASA-sponsored research at: Oak Ridge National Laboratories, the University of North Carolina (Chapel Hill), Sandia Laboratories, Louisiana State University, Communication Satellite Corporation Laboratories, (Clarksburg, Maryland) and the Institute of Energy Conversion of the University of Delaware.

SUMMARY

Single-crystal silicon p-n-junction solar cells made with low-resistivity substrates show poorer solar energy conversion efficiency than traditional theory predicts. The purpose of the research sponsored by grant NSG-3018 is to identify and characterize the physical mechanisms responsible for this discrepancy. Attention concentrates on the open-circuit voltage V_{OC} in shallow-junction cells of about 0.1 ohm-cm substrate resistivity under AMO (one-sun) conditions.

The open-circuit voltage depends on the electronic parameters that characterize the transport, recombination, and generation of electrons and holes in silicon. The many basic mechanisms that can control these electronic parameters are reviewed. Mechanisms contributing to high recombination rates (low lifetime) and large minority-carrier storage (effective gap shrinkage) are identified as the two main origins of the V_{OC} discrepancy in a one-dimensional model of the solar cell. The inadequacies of existing theoretical models and the lack of relevant experimental data and of methods capable of yielding that data prevent an assessment of the relative importance of gap shrinkage and low lifetime in any particular solar-cell structure. Such an assessment is needed to make possible the identification of the basic mechanisms controlling V_{OC}. Thus much of the effort reported here focusses on the development of experimentally-based procedures for determining the effective lifetime and the minority-carrier storage in the quasi-neutral emitter.

A method is described that provides an experimental means for the first time to separate and determine the emitter and base lifetimes in a p-n diode after the junction has been fabricated. In the method, several static and transient measurements are analyzed using physical models of the diode characteristics. To illustrate the method, diffused silicon diodes are fabricated having substrate (base) impurity concentrations ranging from 10^{14} to nearly 10^{17} phosphorous atoms per cubic centimeter. The results show an emitter lifetime that is much smaller than the base lifetime in the diode having the highest base doping concentration. In this diode, the recombination current from the emitter is 65% of the recombination current from the base, demonstrating the significance

of the emitter in governing the static current-voltage dependence. The importance of emitter recombination to the transient characteristics is also demonstrated. The paper emphasizes the techniques by which the base and emitter lifetimes are distinguished. It also demonstrates the need for carefully basing the quantitative analysis of the measurements on the underlying diode physics.

Based on the understanding gained from the study just described, an experimentally-based methodology is then developed that determines the effective gap shrinkage and lifetime in the emitter of a p-n-junction solar cell. It provides the first experimental means available for assessing the importance of gap shrinkage relative to that of large recombination rates in the highly-doped emitter. As an additional result of the procedures employed, the base lifetime is also determined. The methodology pertains to a solar cell after the junction is formed. Hence each material parameter determined includes the effects of the processing used in junction fabrication. The methodology consists of strategy and procedures for designing experiments and interpreting data consistently with the physical mechanisms governing device behavior. This careful linking to the device physics uncovers the material parameters concealed in the data. To illustrate the procedures, they are applied to an n^+-p solar cell having a substrate resistivity of about 0.1 ohm-cm.

The principle of superposition is used to derive from fundamentals the widely used approximation that the current-voltage characteristic of an illuminated solar cell is the dark current-voltage characteristic shifted by the short-circuit current. Thus the derivation requires the linearity of the boundary-value problems that underlie the electrical characteristics. This focus on linearity defines the conditions that must hold if the shifting approximation is to apply with good accuracy. For the solar cell of interest (a 0.1 ohm-cm silicon cell under AMO conditions), the shifting approximation is shown to be valid unless material parameters such as the minority-carrier lifetimes change appreciably under AMO sunlight from the values they have in the dark. Measurements of the dark and illuminated current-voltage characteristics of a 0.1 ohm-cm silicon cell indicate that this does not happen and directly validate

the shifting approximation for such a cell. The theoretical study described here suggests that the shifting approximation will likely be valid for all single-crystal silicon cells under low-injection conditions in the absence of sizable series resistance.

Use of the shifting approximation enables the discrepancy in open-circuit voltage seen in single-crystal silicon cells under AMO conditions to be investigated by studying the electrical behavior of the cell in the dark. Thus it underlies many of the methods and findings described in this report.

CHAPTER I. INTRODUCTION

The solar energy conversion efficiency η of a solar cell is controlled by the product of three factors: the short-circuit photocurrent (I_{SC}), the curve factor or fill factor (FF), and the open-circuit photovoltage (V_{OC}). For high-efficiency silicon p-n-junction cells, the values of FF and I_{SC} approach closely the limits thought to be technologically achievable, but the values of V_{OC} occurring in commercially available silicon cells fall far short of theoretical expectations [1]. Thus the greatest gains possible in η will likely result from increasing V_{OC}.

Figure 1 illustrates the discrepancy between theoretical and experimental V_{OC}. As the substrate (or base) doping concentration N_B increases, the experimentally observed V_{OC} peaks at a substrate resistivity of about 0.1 ohm-cm, corresponding to $N_B \simeq 4 \times 10^{17} cm^{-3}$ for a p-type substrate. This maximum V_{OC} of about 600 mV falls nearly 100 mV below the value of V_{OC} predicted by classical theory for this base resistivity. Removal of this discrepancy in V_{OC} would thus increase η from the maximum of approximately 14% (AMO) now seen [1] to above 17%. Increases of N_B beyond $N_B \simeq 4 \times 10^{17} cm^{-3}$ are unlikely to produce further improvements in η because the minority-carrier base lifetime falls sharply as N_B approaches $10^{18} cm^{-3}$.

The purpose of the research program supported by NASA Grant NSG-3018 is to explain, in fundamental terms, the reasons for the discrepancy that exists between the observed values of V_{OC} and those predicted by traditional theory. The research program concentrates on V_{OC} in (n-on-p) single-crystal silicon p-n-junction solar cells.

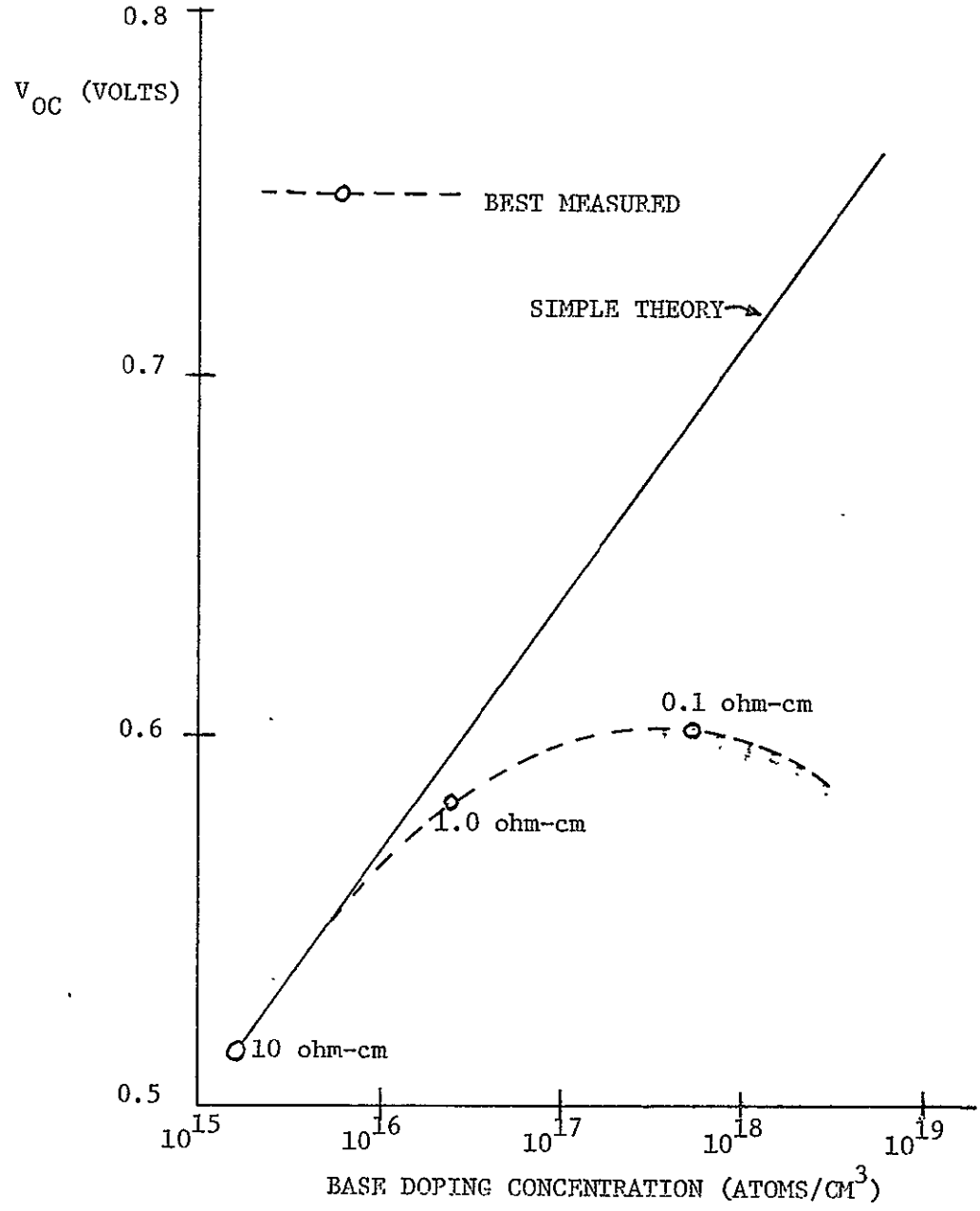

Figure 1: Dependence of open-circuit voltage on base doping concentration. Base resistivity is shown as a parameter.

1.1 Anomalous Values of Minority-Carrier Storage and of Effective Lifetimes in the Emitter

To explore the origin of the V_{OC} discrepancy, note first that the widely-used shifting approximation,

$$I(V) \equiv I_D(V) - I_{SC} \tag{1}$$

provides for 0.1 ohm-cm silicon cells an accurate description under AMO conditions [2]. This approximation views the current-voltage characteristic I(V) of the illuminated cell as the dark characteristic $I_D(V)$ shifted by the short-circuit current I_{SC}. The physical mechanisms occurring in the dark that produce $I_D(V)$ thus become of central importance.

By the principles of charge control,

$$I_D(V) \simeq \frac{Q_E}{\tau_E} + \frac{Q_B}{\tau_B} \tag{2}$$

Here Q_E/τ_E is the recombination current in the quasi-neutral emitter, described as the ratio of excess carrier charge Q_E to the phenomenological lifetime τ_E in the emitter, and Q_B/τ_B is the corresponding recombination current in the quasi-neutral base. At voltages near V_{OC}, the recombination current in the junction space-charge region of silicon cells contributes negligibly to $I_D(V)$ [3-6].

The open-circuit voltage establishes the balance

$$0 = I_D(V_{OC}) - I_{SC} \ . \tag{3}$$

Because I_D, Q_E, and Q_B all increase exponentially with increasing voltage V, the smaller is $I_D(V)$ then the larger will be V_{OC}. Classical theory assumes that $I_D \simeq Q_B/\tau_B$, the emitter recombination current being assumed negligible because the relatively heavy doping concentration in the emitter is assumed to make $Q_E << Q_B$. For AMO conditions, however,

measured values of V_{OC} for a 0.1Ω-cm cell [1-4] imply that $Q_E/\tau_E >> Q_B/\tau_B$. This anomalously large emitter recombination current occurs either because Q_E is larger than is predicted classically, or τ_E is smaller, or for both of these reasons. Various physical mechanisms have been suggested to justify the existence of an anomalously large minority carrier storage or an anomalously small lifetime in the emitter [7,8].

1.2 Order of Presentation

Chapter 2 summarizes the many fundamental electronic mechanisms that could contribute to the anomalous values of minority-carrier charge storage and lifetime. Chapter 3 concentrates on lifetime. It describes methods that enable for the first time the determination by electrical measurements of the phenomenological lifetime τ_E in the emitter. The methods give also the value of the base lifetime and identify and characterize the imperfection centers in the base. In Chapter 4, the methods are extended so that they yield not only the phenomenological lifetime τ_E but also the minority-carrier charge storage Q_E in the emitter. The application of these methods to an n^+-p junction solar cell having a base resistivity of about 0.1 ohm-cm indicates that Q_E is larger than conventional theory predicts and that τ_E is smaller than the base lifetime τ_B. As discussed in Chapter 5, these new experimental methods will serve several purposes in our future research. They help toward determining which of the many possible fundamental electronic mechanisms dominate in degrading V_{OC}. They help enable a better estimate of the maximum η achievable from silicon technology. They provide a basis for studies aimed to increase V_{OC} and hence η.

The approaches of Chapters 3 and 4 require the validity of the shifting approximation of (1), which implies that a study of the dark current-voltage characteristic $I_D(V)$ will suffice in determining the origin of the V_{OC} discrepancy. Fundamental considerations underlying the validity of (1) are treated in the Appendix.

Insofar as is possible, each of the Chapters are written as independent units to enable the reader with a main interest in a later chapter to be able to read that one directly without first having to become familiar with the earlier chapters.

REFERENCES FOR CHAPTER 1

1. W. Shockley, "The Theory of p-n Junctions in Semiconductors and p-n Junction Transistors," Bell Sys. Tech. J., vol. 28, pp. 435-489, July 1949.

2. F. A. Lindholm, J. G. Fossum, and E. L. Burgess, "Basic Corrections to Solar Cell Performance Required by Inapplicability of Superposition," Record of Twelfth Photovoltaic Specialists Conf., paper 2.5, Nov. 1976.

3. F. A. Lindholm, C. T. Sah, A. Neugroschel, M. P. Godlewski, and H. W. Brandhorst, "Methodology for Experimental Determination of Gap Shrinkage and Lifetimes in Emitter and Base of pn Junction Solar Cells," Record of Twelfth Photovoltaic Specialists Conf., paper 1.1, Nov. 1976.

4. F. A. Lindholm, A. Neugroschel, and C. T. Sah, "Junction Modeling for Solar Cells--Theory and Experiment," Tech. Digest 1976 Int. Electron Devices Meeting, 76CH1151-0ED, pp. 61-65, Dec. 1976 (invited paper).

5. F. A. Lindholm, A. Neugroschel, C. T. Sah, M. P. Godlewski, and H. W. Brandhorst, Jr., "Methodology for the Experimental Determination of Gap Shrinkage and Lifetimes in the Emitter and Base of p-n-Junction Diodes and Solar Cells," IEEE Trans. Electron Devices, April 1977.

6. A. Neugroschel, F. A. Lindholm, and C. T. Sah, "A Method for Determining the Emitter and Base Lifetimes in p-n-Junction Diodes," IEEE Trans. Electron Devices, June 1977.

7. F. A. Lindholm and C. T. Sah, "Fundamental Electronic Mechanisms Limiting the Performance of Solar Cells," IEEE Trans. Electron Devices, April 1977.

8. C. T. Sah and F. A. Lindholm, "Carrier Generation, Recombination, Trapping and Transport in Semiconductors with Position-Dependent Composition," IEEE Trans. Electron Devices, April 1977.

CHAPTER II. FUNDAMENTAL ELECTRONIC MECHANISMS LIMITING THE PERFORMANCE OF SOLAR CELLS

I. Introduction

Any attempts to characterize the efficiency of solar cells from a fundamental viewpoint must begin with a set of differential equations that describe the transport, recombination, and generation of holes and electrons. The efficiency obtainable from different material technologies depends upon the fundamental limitations imposed on the material parameters appearing in these equations. The various basic mechanisms that can determine the properties of these material parameters are the main subject of this paper.

In the sections to follow, two dominant mechanisms are discussed: (a) distortion in the energy band, and (b) carrier recombination and generation rates or lifetimes. The spatial dependences associated with these mechanisms are emphasized--both in the direction normal to the surface on which the sun shines and that tangential to it. As will be seen, the spatial dependences can play a central role in determining the solar cell efficiency.

II. Basic Mechanisms Affecting Conversion Efficiency

2.1 The Shockley Equations

The basic mechanisms that determine the efficiency of a solar cell can be analyzed from the basic set of differential equations that govern the transport and recombination-generation-trapping of the electrons and holes in a semiconductor. These equations were first used by Shockley [1] for thermal recombination and generation of electrons and holes. They were generalized by Sah [2] to include optical and other generation-recombination processes and further extended to

include high recombination-generation or low scattering rates [3] using the Boltzmann equation. The complexities introduced by varying material composition and heavy impurity doping, resulting in positional dependent electron affinity and energy gap, were also discussed and analyzed by Van Overstraeten [4], but the significance of band and bound states separated by a mobility edge was not recognized. The concept of a mobility edge will be further elaborated on in a later section and in a companion paper [5]. For the present purpose of delineating the important solar cell parameters, the Shockley equations for the specialized condition of d.c. steady-state in compositionally uniform material will suffice. These are [2]:

$$\vec{J}_N = +qD_n \nabla N + q\mu_n N\vec{E} \tag{1}$$

$$= - q\mu_n N \nabla V_N \tag{1a}$$

$$\vec{J}_P = - qD_p \nabla P + q\mu_p P\vec{E} \tag{2}$$

$$= - q\mu_p P \nabla V_P \tag{2a}$$

$$0 = + \nabla \cdot J_N + I_{SS} \tag{3}$$

$$0 = - \nabla \cdot \vec{J}_P + I_{SS} \tag{4}$$

$$\nabla \cdot \vec{E} = - \nabla^2 V_I = \rho/\varepsilon = (q/\varepsilon)(P - N + N_{DD} - N_{AA} - N_T) \tag{5}$$

They can be solved for any device geometry and material parameters, as part of a boundary-value problem, using the auxiliary conditions

$$N = n_i \exp[q(V_I - V_N)/kT], \tag{6}$$

$$P = n_i \exp[q(V_P - V_I)/kT] \tag{7}$$

and the boundary conditions to give the total current and applied voltage, V_A,

$$\vec{J} = \vec{J}_N + \vec{J}_P, \quad V_A = V_P(0) - V_N(L) \tag{8}$$

as a function of such external excitations as the light intensity. In the expression for the applied voltage given by (8), the ohmic contact to the p-type is located at x=0 and to the n-type is located at x=L.

Equation (1) expresses the electron current density, $\vec{J}_N$ in A/cm^2, as the sum of a diffusion component, which is proportional to the gradient of the concentration of the electrons, N, and a drift component, which is proportional to the conductivity, $q\mu_n N$, and the electric field, $\vec{E}$. The coefficient of proportionality involves the electron mobility, μ_n, and diffusivity, D_n. Equation (1a) gives an equivalent way of expressing the electron current density, in terms of the product of the electron conductivity, $q\mu_n N$, and the gradient of the quasi-Fermi potential of electrons, V_N.

Equations (2) and (2a) are the hole current expressions; they are similar to those given in Equations (1) and (1a) just described for electrons.

The physical basis for the definition of carrier mobilities and diffusivities appearing in Equations (1) to (2a) is a nontrivial one when the band and bound states are not separated by a distinct energy band edge. Such a fuzzy band edge occurs in heavily doped single crystal and polycrystalline semiconductor materials for solar cell applications. A mobility edge is then defined to delineate the band states of high carrier mobility from bound states of low or negligible carrier mobility. The latter must then be taken into account as carrier generation-recombination-trapping centers to be included in Equations (3) and (4). This is further elaborated on in a later section. (See also Sah [5].)

Equations (3) and (4) are the continuity equations for electron and hole currents. They state that the dc steady state is maintained by two components

so that there is no time dependence of electron or hole concentrations. These two components are the divergence of the electron or hole current density and the net steady-state generation (generation minus recombination) of electrons and holes. The latter is written as a volume current source, I_{SS}. It consists of all the contributions from the many possible electron-hole generation and recombination mechanisms which have been described in detail by Sah [2]. For this discussion, we shall decompose I_{SS} into components particularly important for solar cell applications, which can be written as

$$I_{SS} = q(G_N^O - R_N) = q(G_P^O - R_P) \qquad (9)$$

Here, G_N^O and G_P^O are the optical generation rate of electrons and holes respectively. They are equal, $G_N^O = G_P^O = G^O$, if we consider only the interband optical generation of electron-hole pairs from photoexcitation of electrons in the valence band into the conduction band and neglect optical excitation of electrons and holes trapped at impurity and defect centers. R_N and R_P are the net recombination rates of electrons and holes, respectively.

In solar cells, the term G^O describes the generation of electron-hole pairs by sunlight. It gives rise to the total photocurrent or short circuit current, J_{SC}, which is commonly used to characterize the quality of a solar cell and to guide in the design of efficient solar cells. [6]

If only the interband optical generation of electron-hole pairs is considered as indicated above, then we have the simple steady-state condition $R_N = R_P = R_{SS}$. The net steady-state recombination rate, R_{SS}, contains nonoptical and nontunneling mechanisms discussed by Sah [2]. These mechanisms are band and band-bound thermal and Auger-impact transitions which are summarized below for the d.c. steady-state condition.

$$R_{SS} = R^{T}_{CV} + R^{A}_{CV} + R^{T}_{CTV} + R^{A}_{CTV} \tag{10}$$

The band-to-band (conduction-valence band) net steady-state recombination rates are:

$$R^{T}_{CV} = q(r^{t}NP - g^{t}) \qquad \text{Thermal} \tag{11}$$

$$R^{A}_{CV} = (r^{n}N^{2}P - g^{n}N) + q(r^{p}P^{2}N - g^{p}P) \qquad \text{Auger-Impact} \tag{12}$$

which can be combined to give

$$R_{CV} = R^{T}_{CV} + R^{A}_{CV} = q(rNP - g) \tag{13}$$

where

$$r = r^{t} + r^{n}N + r^{p}P, \qquad g = g^{t} + g^{n}N + g^{p}P \tag{14}$$

Here, r^{t} and g^{t} are the interband thermal recombination and generation rates of electron-hole pairs. r^{n} is the Auger recombination rate of an electron-hole pair in which the energy is carried away by an electron while g^{n} is the impact generation rate of an electron-hole pair initiated by an energetic electron. r^{p} and g^{p} have the same meaning but the third particle is a hole.

The net steady-state recombination rate for band-bound or conduction band-trap-valence band transitions consists of that for the thermal mechanism, $R^{T}_{CTV} \equiv R_{SRH}$ first considered by Shockley, Read and Hall [7], and the Auger-Impact mechanism, R^{A}_{CTV}. The net d.c. steady-state rate of these two mechanisms for single-level generation-recombination-trapping (GRT) center is given by [2]

$$R_{CTV} = R^{T}_{CTV} + R^{A}_{CTV} = qN_{TT}\frac{c_{n}c_{p}NP - e_{n}e_{p}}{c_{n}N + e_{n} + c_{p}P + e_{p}} \tag{15}$$

and the trapped charge concentration, N_T, is given by

$$\frac{N_T}{N_{TT}} = \frac{c_n N + e_p}{c_n N + e_n + c_p P + e_p} \tag{16}$$

The capture and emission coefficients are given by

$$\begin{aligned} c_n &= c_n^t + (c_n^n N + c_n^p P), \quad e_n = e_n^t + (e_n^n N + e_n^p P) \\ c_p &= c_p^t + (c_p^n N + c_p^p P), \quad e_p = e_p^t + (e_p^n N + e_p^p P) \end{aligned} \tag{17}$$

Here, c_n^t and c_p^t are the thermal capture rates and e_n^t and e_p^t are the thermal emission rates of electrons and holes respectively at a single level GRT center whose positional dependent concentration is denoted by $N_T(x,y,z)$. c_n^n is the Auger capture rate of an electron by a trap with a second electron carrying away the energy while c_n^p is the Auger capture rate of an electron by a trap but with a hole carrying away the energy. The rates of the corresponding inverse transition processes of trapped electrons are denoted by e_n^n and e_n^p, with the superscripts denoting the energetic electron, n, or hole, p, which cause the impact emission transition of a trapped electron. The corresponding rate coefficients for Auger capture and impact emission of a hole are denoted by c_p^p, c_p^n, e_p^p and e_p^n.

Equation (5) is the Poisson equation which relates the electric field, $\vec{E}$, and electrostatic potential, V_I, in the solar cell to the macroscopic charge concentrations. The components of the charge concentrations include the concentrations of the ionized donors and acceptor impurities, N_{DD} and N_{AA}, which may be position-dependent, as well as the concentration of the negatively charged GRT centers, N_T, given by Equation (16). In many of the earlier mathematical analyses of semiconductor devices, the trapped charge, $-qN_T$, is neglected. For example, Shockley's p-n junction theory [1] did not include the trapped charges in the

Poisson equation when it was solved to obtain the electrostatic potential in the junction. A detailed analysis of the d.c. steady-state trapped charge concentration, such as Equation (16), was later given by Shockley and Read in their work on recombination kinetics [7] where detailed analyses of the effect of trapping on the steady-state lifetimes were given in the appendix. The importance of the trapped charge can be simply illustrated by noting that near the p-n boundary of a junction, $N_{DD}-N_{AA}$ is nearly zero so that the trapped charge, N_T, can have a substantial effect on the electrostatic potential variation in materials with non-negligible trap concentration such as solar-grade silicon single crystals and polycrystalline films.

These equations, together with appropriate boundary conditions, can determine all aspects of solar cell operation, including solar cell energy conversion efficiency. To help achieve better conversion efficiency a quantitative understanding is needed of the material parameters appearing in the equations, and particularly of the functional dependencies of these parameters. In essentially all previous simple analyses of solar cells, as well as in detailed numerical computer solutions of these equations for solar cells, many idealizing approximations for the parameters have been made, for example, the recombination rates R_N and R_P. These approximations were made and then propagated to later work for three apparent reasons. First, they simplified analysis. Second, the severity of approximation involved has apparently gone unrecognized, except in a few instances, and the approximations have been treated as if they were valid. Third, and most important, experimental tools have not been developed and applied to supply the needed functional dependencies of these parameters in solar cell structures.

The functional dependencies of the material parameters therefore govern solar cell efficiency. The dependencies have their physical origin in certain basic mechanisms as well as in cell inhomogeneities. Among the most important of these are:

(1) Distorted energy bands,

(2) Interband or band-bound transition or recombination rates, and

(3) Positional dependences in directions normal and parallel to the illuminated surfaces (areal inhomogeneity).

We now briefly discuss these factors and their role in determining solar cell conversion efficiency for various material systems.

2.2 Distorted Energy Bands

At high doping concentrations, and for material with considerable disorder, such as polycrystalline films or varying chemical composition, various deviations from the idealized band structure can occur, such as:

(1) The energy band edges are no longer sharp. Electronic energy levels can extend beyond the energy positions of band edges of perfect single-crystal material, forming thereby so-called band tails [8];

(2) The localized impurity states can broaden into an impurity band [9] with increasing impurity concentration. At high doping levels, these states can become substantially delocalized;

(3) A spatial variation of the energy gap can result from macroscopic lattice strain introduced by a high-concentration diffused impurity and structural imperfection in the lattice [10], as well as chemical composition variation in graded materials [5, 11] and hetrojunctions [12].

Each of these deviations tends to produce an effective shrinkage ΔE_G of the energy band gap. Because the intrinsic density n_i depends exponentially on the band gap, the gap shrinkage has been imbedded, as a first-order approximation, in an effective intrinsic density [13], which then appears directly in Eqs. (6) and (7). Note that spatial dependence of the doping concentration implies spatial dependence of the effective band gap.

To examine qualitatively the effect of gap shrinkage on the conduction processes described in Eqs. (1) and (2) and on the recombination-generation rate in Eqs. (3) and (4), we must distinguish whether the electronic states in the presence of high doping are localized or delocalized. Thus, borrowing from the concepts used in models describing amorphous semiconductors, we identify a critical energy, the Cohen mobility edge [14], which separates localized states from delocalized states. The mobility edge plays a dominant role in describing charge transport in disordered-aperiodic solids similar to the role the band edge plays in periodic solids such as lightly-doped silicon.

For delocalized states, conduction can occur by drift and diffusion. If the variation in doping produces spatial dependence of the band gap and the electron affinity, the so-called quasi-electric fields [5,11] produces the drift currents of electrons and holes. For localized states, conduction can occur by carrier hopping between neighboring states [15] due to thermally activated transfer of the trapped charges in the Mott model [16] or by tunneling in the Anderson model [17].

For ordinary temperatures encountered in solar cell operations, only the delocalized or band states will have high carrier mobility and dominate the electrical current. In these band states, three effective forces may act to produce the flow of electrons and holes. They are: (i) the Coulomb and short-range forces, giving rise to the diffusion current due to concentration gradient, (ii) the electric force, giving rise to the conventional drift current and (iii)

the electric force from the positional dependences of energy gap and electron affinity, giving rise to additional drift currents. The second and third effective force can be combined into an electric field known as the quasi-electric field whose gradient gives the drift current components [5]. The total current written in terms of the gradient of the quasi-Fermi potentials given by Equations (1a) and (2a) remain valid as they give zero currents at equilibrium when the quasi-Fermi potentials coincide and become spatially constant.

2.3 Interband and Band-Bound Transitions: Recombination Rates and Effective Lifetimes

The interband and band-bound transition rates of electrons and holes, R_N and R_P given in Equation (9), are customarily modeled using oversimplified approximations in semiconductor device analysis. For example, they are normally written as the excess carrier concentration (nonequilibrium minus equilibrium carrier concentration) divided by a constant effective lifetime. This constant recombination lifetime model is questionable in the diffused emitter layer of single-crystal silicon junction and is likely to be too simplified for polycrystalline solar cell materials in general. For instance, the transition rates or the effective lifetimes of electrons and holes depend on the several energy-momentum conservation mechanisms such as the phonon-assisted or thermal, the photon-assisted or optical and the three-body or Auger-Impact processes. [2] The recombination rates of such transitions depend on the density, the energy levels and the electron and hole capture and emission rates of the localized centers, and on the positional dependences of the energy band gap. These rates have already been summarized in Equations (10) to (17). Only under rather special circumstances, namely low illumination and extremely high illumination intensities, can these rates be characterized by constant

lifetime provided the concentrations of the recombination centers are spatially constant [6]. The lack of spatial variations is most unlikely in polycrystalline solar cells but also in single crystal cells in view of its large geometry as well as the heavily disordered diffused layer. A major reason for the use of the constant lifetime approximation in the past was the unavailability of accurate experimental data on the recombination parameters and the lack of sensitive experimental techniques which can determine these parameters in solar cells instead of the uniform semiconductor bulk. New methods have now been developed so that one can measure these parameters in solar cell structures [6, 18, 19].

Aside from the mechanisms mentioned, another type exists that can influence the effective interband transition rates. This involves the tunneling transition via deep-level defect centers [2]. Among the many transition processes of this general type [20], we shall describe here a particular two-step process. This process assumes that an electron in the conduction band is first captured by a localized deep level and subsequently tunnels to the valence band or to the valence-band tail states. It has been demonstrated experimentally that this is the excess-current mechanism in gold-doped silicon tunnel diodes [21].

In polycrystalline films, recombination processes occur at grain boundaries by any of the energy/momentum conservation mechanisms mentioned previously. As a phenomenological first-order approximation, one can characterize this recombination in terms of an effective surface recombination velocity S acting over the surface area of the grain boundaries. Choice of various assumed structures of the grains can then enable theoretical study, for example, of the relation between the size of the grain and the effective lifetime of the polycrystalline material. [22]

2.4 Spatial Dependences

The effect of the mechanisms just discussed on the solar-cell efficiency depends critically on the spatial dependences of these mechanisms in the direction normal to the surface of the cell, as well as in the transverse direction. These are discussed in the following two sections.

Variations Normal to the Cell Surface

The shrinkage of the energy gap may become large in regions that are heavily doped, for example, in the diffused emitter region of a pn junction solar cell. There it acts to increase the minority charge stored. The spatially variation impurity concentration in the diffused emitter will also produce a built-in electric field which can reduce the transit time required for the minority carriers to cross the emitter region. Both of these effects tend to increase the dark saturation current, thus lowering the open-circuit voltage and the conversion efficiency.

In the heavily-doped emitter of a p-n junction solar cell, one expects the defect density to rise sharply near the degenerately-doped surface. This expectation comes from the experimental evidence [23] on single-crystal silicon which showed that during silicon device processing, recombination centers are generated at the strained and disordered surface layer and diffuse rapidly into the bulk.

These experiments further suggest that the centers are silicon vacancies or vacancy complexes. Thus, using the analogy to chemical reactions reviewed by Fuller [24], one finds the following first-order model for the dependence of the recombination center density N_{TT} on the concentration of the impurity N_{DD} in the diffused emitter and space-charge regions:

$$N_{TT}(x) = K[N_{DD}(x) + N_{AA}]^{r}.$$

In developing this model, one assumes approximate thermal equilibrium during the diffusion of impurities. This justifies the law of mass action, which one combines with the electrical neutrality condition. The different values of r are

derived from different hypotheses about the dominant chemical reaction. For reactions corresponding to the formation of divacancies, the choice r = 2 provides an approximate fit. Experimental techniques exist [6] by which one can study the validity of the theoretical anticipation given in Equation (18), and determine the value of the parameter r if the theoretical anticipation is valid for the cell under study.

The occurences of spatial dependences and high concentrations of recombination centers would degrade solar cell performance in various ways. High recombination rate in the junction space-charge region and in quasi-neutral emitter layer of p-n junction solar cells increase the dark saturation current and thereby lower the open-circuit voltage. Moreover, recombination in the space-charge region, where electron and hole concentrations are large, tends to decrease the fill factor as well as the short circuit current [6]. Thus, high recombination rates in the junction space-charge region and in the quasi-neutral emitter act in three ways to decrease the conversion efficiency. In addition, if the lifetime in the quasi-neutral base were to decrease with position in the direction toward the surface, then the dark saturation current would further increase. Hence, this too can contribute to lowering the conversion efficiency.

Variation Across Surface (Areal Inhomogeneity)

We have thus far considered a one-dimensional model of the cell in which the only coordinate of interest has been that measuring the distance from the surface. But the solar cell is a large-area device, and inhomogeneities across its area could play a significant role in governing the performance. In particular, we note the existence of a spatial distribution of impurity clusters, thermodynamically stable, occurring in heavily-doped emitter regions [25]. Thus, the inhomogeneities may result, in part, from inescapable statistical fluctuations and, in part, from man-made contributions that could be minimized.

One can systematically view the influence of the one-dimensional mechanisms discussed previously in the context of inhomogeneity across the area of the cell. We stress that the overall effect on solar cell characteristics is not a simple average over the area of the cell. Indeed, a small defective area could dominate in determining the conversion efficiency of a large area solar cell. For example, certain of the mechanisms are much emphasized in a region of large-impurity concentration due to clustering. An example is energy band gap shrinkage, which enters as an exponent in determining cell properties in a localized region; another example is the associated increased defect density and the increased recombination rates corresponding to it. The model of a solar cell as a collection of mini-cells connected in parallel with one another, although much simplified, qualitatively suggests the trends in behavior introduced by areal inhomogeneity: that those mini-cells with relatively high doping or defect density (or with small grain size in a polycrystalline film) can severely degrade the performance of the device. Hence, areal inhomogeneity could play a dominant role and establish a technological limitation on the solar conversion efficiency obtainable.

III. SUMMARY

Certain basic mechanisms in semiconductor material and their dependence on position were the subjects of this paper. In outline form, the subjects treated were:

(a) Distorted and spatially varying energy band in highly-doped and variable chemical composition material

(b) Bulk, surface and grain boundary recombination

(c) Spatial dependencies normal to the surface and areal inhomogeneities

Each of the above can strongly influence the performance of solar cells. For example, energy band distortion present in a highly-doped emitter can limit the open-circuit voltage obtainable in p-n junction solar cells. High recombination rates can affect the short-circuit current, the fill factor, and the open-circuit voltage. The spatial dependence of the energy band distortion and the recombination rates, both across the area of the cell and in the direction normal to the surface, can determine the degree to which the fill factor, the short-circuit current, and the open-circuit voltage are degraded. Recently, experimental methods have been developed and applied to silicon solar cells to determine the species of recombination centers [6] and the energy gap shrinkage and the effective lifetime in the heavily-doped emitter [19].

All of the mechanisms above apply both to single-crystal as well as to polycrystalline thin-film materials. For polycrystalline cells, processes at grain boundaries can play a central role in determining the solar conversion efficiency [22].

Research studies are needed to improve our understanding of the basic mechanisms treated here. Detailed quantitative studies are required to assess the ultimate capabilities of any particular material technology. Thus such research can potentially yield a basis for choosing from among alternative technologies. Moreover, for solar cells made from any given technology, such as the technology of single-crystal silicon, studies of the basic mechanisms can help guide the fabrication processing toward maximizing the conversion efficiency.

In chapters 3 and 4, we describe studies of silicon devices that help toward achieving all of these objectives.

REFERENCE FOR CHAPTER 2

[1] W. Shockley, "The theory of p-n junctions in semiconductors and p-n junction transistors," Bell Syst. Tech. J., vol. 28, pp. 435-489, 1949.

[2] C. T. Sah, "Equivalent circuit models in semiconductor transport for thermal, optical, Auger-impact, and tunneling recombination-generation-trapping processes," physica status solidi a, vol. 7, pp. 541-559, 1971.

[3] C. T. Sah and F. A. Lindholm, "Transport in semiconductors with low scattering rate and at high frequencies," Solid-State Electronics, vol. 16, pp. 1447-1449, 1973.

[4] R. J. Overstraeden, H. J. DeMan and R. P. Mertens, "Transport equations in heavy doped silicon," IEEE Trans. Electron Devices, vol. ED-20, pp. 290-298, 1973.

[5] C. T. Sah, "Carrier generation, recombination, trapping and transport in semiconductors with position dependent composition," IEEE Trans. Electron Devices, this issue.

[6] C. T. Sah, "Detection of recombination centers in solar cells from capacitance transients," IEEE Trans. Electron Devices, this issue.

[7] W. Shockley and W. T. Read, Jr., "Statistics of the recombinations of holes and electrons," Phys. Rev., vol. 87, pp. 835-842, 1952.

[8] I. M. Lifshitz, J. Exp. Theor. Phys., vol. 2, pp. 117, 137, 156, 1942.

[9] G. W. Castellan and F. Seitz, "The transition from insulating to metallic behavior in semiconducting silicon," Phys. Rev., vol. 79, pp. 216-222, 1950; C. S. Hung, "Theory of resistivity and Hall effect at very low temperature," Phys. Rev., vol. 79, pp. 727-728, 1950; C. Erginsoy, "On the mechanism of impurity band conduction in semiconductors," Phys. Rev., vol. 80, pp. 1104-1108, 1950; and T. N. Morgan, "Broadening of impurity

bands in heavily doped semiconductors," Phys. Rev., vol. 139A, pp. A343-A348, 1965.

[10] V. Fistul, Heavily Doped Semiconductors, Plenum Press, N.Y., 1969.

[11] H. Kroemer, "Band structure of semiconductor alloys with locally varying composition," Bull. Amer. Phys. Society, vol. 1, p. 143, Paper V9, 1956; "Quasi-electric and quasi-magnetic fields in nonuniform semiconductors," RCA Review, vol. 28, pp. 332-342, 1957.

[12] A. G. Milnes and D. L. Feucht, Heterojunctions and Metal-Semiconductor Junctions, Academic Press, 1972.

[13] D. D. Kleppinger and F. A. Lindholm, "Impurity concentration dependence of the density of states in semiconductors," Solid-State Electronics, vol. 14, pp. 199-206, 1971; D. D. Kleppinger and F. A. Lindholm, "Impurity concentration dependent density of states and resulting Fermi level for silicon," Solid-State Electronics, vol. 14, pp. 407-416, 1971; H. J. DeMan "The influence of heavy doping on the emitter efficiency of a bipolar transistor," IEEE, vol. ED-13, pp. 833-834, 1971; R. J. Van Overstraeten, H. J. DeMan, and R. P. Mertens, "Transport equations in heavy doped silicon," IEEE. vol. ED-20, p. 290, 1973; H. J. DeMan, R. P. Mertens and R. J. Van Overstraeten, "Influence of heavy doping effects on the f_T prediction of transistors," Electronic Letters, vol. 9, pp. 248-249, 1973; R. P. Mertens H. J. DeMan and R. J. Van Overstraeten, "Transport equations in heavy doped silicon," IEEE Trans. Electron Devices, vol. ED-20, pp. 772-778, 1973; M. S. Mock, "Transport equations in heavily doped silicon, and the current gain of a bipolar transistor," Solid-State Electronics, vol. 16, pp. 1251-1259, 1973; M. S. Mock, "On heavy doping effects and the injection efficiency of silicon transistors," Solid-State Electronics, vol. 17, pp. 819-824, 1974; and M. P. Godlewski, H. W. Brandhorst, Jr., and C. R. Baraona, "Effects of high doping levels on silicon solar cell performance," High Efficiency

Silicon Solar Cell Meeting, NASA-Lewis Research Center, 1974; Record of 11th Photovoltaic Specialists Conf., pp. 32-36, 1975.

[14] M. H. Cohen, H. Fritzsche, and S. R. Ovshinsky, "Simple band model for amorphous semiconducting alloys," Phys. Rev. Lett., vol. 22, pp. 1065-1068, 1969.

[15] E. M. Conwell, "Impurity band conduction in germanium and silicon," Proc. IRE, vol. 103, pp. 51-61, 1956.

[16] N. F. Mott, "On the transition to metallic conduction in semiconductors," Can. J. of Physics, vol. 34, pp. 1356-1368, 1956.

[17] P. W. Anderson, "Absence of diffusion in certain random lattices," Phys. Rev. vol. 109, pp. 1592-1605, 1958.

[18] C. T. Sah, L. Forbes, L. L. Rosier, and A. F. Tasch, "Thermal optical emission and capture rates and cross sections of electrons and holes at imperfection centers in semiconductors from photo and dark junction current and capacitance experiments," Solid-State Electronics, vol. 13, pp. 759-788, 1970; For a review of the applications of these techniques to recombination centers in silicon, see C. T. Sah, "Bulk and interface imperfections in semiconductors," Solid-State Electronics, vol. 20, pp. 1-20, 1976. See also reference 5.

[19] (a) F. A. Lindholm, A. Neugroschel, C. T. Sah, M. P. Godlewski, and H. W. Brandhorst, Jr., "Methodology for the experimental determination of gap shrinkage and lifetimes in the emitter and base of pn-junction solar cells," IEEE Trans. Electron Devices, this issue; also Record of 12th Photovoltaic Specialists Conf., Nov. 1976.

(b) F. A. Lindholm, A. Neugroschel, and C. T. Sah, "Junction modeling for solar cells — theory and experiment," Digest of 1976 Int. Electron Devices Meeting, Dec. 1976.

(c) A. Neugroschel, F. A. Lindholm, and C. T. Sah, "A method for determining the emitter and base lifetimes in pn-junction diodes," IEEE Trans. Electron Devices, submitted for publication.

[20] C. T. Sah, "Excess current in semiconductor tunneling," in Tunneling Phenomena in Solids, Ch. 14, (Editors: E. Burstein and S. Lindquist) Plenum Press, N.Y., 1969.

[21] C. T. Sah, "Electronic processes and excess currents in gold-doped narrow silicon junctions," Phys. Rev. pp. 1594-1612, 1961.

[22] C. T. Sah and F. A. Lindholm, "Characteristics of solar cells on granular semiconductors," Proceedings of the 12th IEEE Photovoltaic Specialists Conference, Nov. 15, 1976.

[23] C. T. Sah and C. T. Wang, "Experiments on the origin of process induced recombination centers in silicon," J. Appl. Phys., vol. 46, pp. 1767-1776, 1975.

[24] C. S. Fuller in Semiconductors, Ch. 5, (Editor: N. B. Hannay) Reinhold Corp., N.Y., 1959.

[25] W. Shockley, "Problems related to p-n junctions in silicon," Solid-State Electronics, vol. 2, pp. 35-67, 1961.

CHAPTER III. A METHOD FOR DETERMINING THE EMITTER AND BASE LIFETIMES

I. INTRODUCTION

Past work on p-n-junction diodes has not provided a means for the experimental determination of the emitter lifetime. This has prevented a quantitative assessment, based on experiment, of the importance of carrier recombination in the emitter to the electrical characteristics of p-n diodes, solar cells, and bipolar transistors.

A main purpose of this paper is to emphasize and to demonstrate, *by experiment*, the significance of the heavily-doped emitter region of a diode to its forward current-voltage characteristics. The experimental evidence to be presented shows that the emitter can play a significant role in the response to both static and transient excitations. In the course of the study, the minority-carrier lifetimes are found experimentally for the emitter and the base regions. As will be seen, the determination of these two lifetimes demands that more care be given to constructing experiments and interpreting experimental evidence than has been given previously. A second main purpose of this paper is to describe the techniques by which we distinguish the emitter lifetime from the base lifetime.

The reference to emitter and base used above for diodes borrows the terminology used for transistors. In the paper, this terminology will refer to a p-n diode consisting of a heavily-doped p-type emitter and an n-type base that is more lightly doped. The emitter and base are quasi-neutral regions separated from each other by the space-charge region of the junction. For concreteness the treatment throughout this paper will refer to a p^+-n structure; an analogous treatment applies for n^+-p structures.

The significance of the emitter applies not only to diode theory but also to the theory of operation of other devices, such as the p-n junction solar cell and the bipolar transistor, whose structure involves one or more p-n junctions. For example, the physical processes occurring in the emitter of a bipolar transistor can limit the achievable maximum common-emitter current gain. For the p-n junction solar cell, as Chapters 1 and 2 have discussed, these processes can limit the achievable maximum solar energy conversion efficiency. The experiments and particularly the methods for interpreting experimental data treated in this paper for diodes, therefore, apply also to junction transistors and solar cells. A key connection between p-n-junction diodes and p-n-junction solar cells is the shifting approximation (Eq. 1, Ch. 1), the validity of which forms the subject of the Appendix.

The emitter will be significant to the behavior of a device whenever the current that supports the recombination in the emitter constitutes an appreciable fraction of the currents flowing at the device terminals. A large emitter recombination current arises from high recombination rates in the emitter. As has been discussed in Chapter 2, such rates can be traced to various physical origins, which fall into two broad categories [1]:

(a) *band-edge distortion* that may be present in heavily-doped material can affect recombination, diffusion and drift; and

(b) crystalline imperfections, formed near the emitter surface and diffused into the emitter during high-temperature fabrication, can act as *recombination centers*, producing a lower lifetime in the emitter than in the base.

The effect of recombination in the emitter, category (b) above, receives the emphasis in this paper. The design of the diode structures used here purposefully makes negligible the effects of band-edge distortion. Chapter 4 will treat the effects of band-edge distortion, category (a) above.

Section II gives details about the design and fabrication of the diodes. Section III gives the values of the recombination-generation parameters of the deep energy levels present in the base, as revealed by transient-capacitance experiments. The energy levels studied in detail fall in the upper half of the bandgap. These energy levels control the lifetime of minority carriers in p-type material. Thus studies of the type reported here, made on p-on-n diodes,can potentially yield the parameters controlling and limiting the base lifetime in n-on-p solar cells. This relationship is noted because n-on-p solar cells show advantages for space applications, and are the type of cell of main interest in this NASA grant research.

Section IV characterizes the static current-voltage dependence in a way that is consistent with the underlying physics. Such a characterization is essential to the proper calculation of values of lifetimes and of other material properties. Section V demonstrates and discusses erroneous conclusions about the base lifetime calculated from improper current-voltage characterizations used in the past. In Section VI, methods for interpreting data are described that distinguish the material properties of the emitter from those of the base. Applying these methods then yields the values for the lifetimes of the emitter and the base, which are tabulated and discussed in Sections VI and VII.

II. DIODE FABRICATION AND PHYSICAL MAKE-UP

Boron was diffused into n-type silicon substrates of (111) orientation to form p^+-n junctions. Four sets of diodes were made, each with a different phosphorous concentration N_{DD} in the substrate, ranging from 10^{14} to 10^{17} cm^{-3}.

Various substrate doping concentrations were used to permit the testing of qualitative expectations about the significance of the emitter. On qualitative grounds, one notes, for example, that the excess minority charge stored in the base is inversely proportional to the doping concentration of

the base (substrate), as a first approximation. Hence the higher the substrate doping the more one might expect the emitter to dominate the current-voltage characteristics of the diode. This expectation is borne out by the experimental results described in Sections V and VI.

In the fabrication of the diodes, after standard surface cleaning [2], a 0.5 μm thick oxide layer was grown in a wet oxygen ambient. Holes of rectangular area 25x42 mil^2 were opened in the oxide on the top surface using standard photolitographic techniques. Boron was then predeposited into these oxide holes from a solid planar Boron-plus source at 1100°C for 30 minutes in mixed $N_2 + O_2$ carrier gas. The boron glass was then etched away and a boron drive-in diffusion was done at 1200°C for three hours in dry oxygen.

Slow pulls lasting about 5 min. were used during the predeposition step, mainly to avoid thermal warpage of the diffusion sources. The pull rate was high during the drive-in step. For the studies of interest here, pull rates are not very important since only extremely slow cooling could reduce the recombination-center densities in the bulk [3].

Contact holes to the p^+ region were then opened in the 0.35 μm oxide layer grown during the drive-in step. Aluminum was evaporated on the top side and was selectively removed using photolitrography to define contacts to the p^+ region and to create an MOS guard-ring gate overlapping the edge of the diffused layer. Aluminum contacts were sintered at 450° for 30 minutes in dry N_2. The back side was lapped to assure a good ohmic contact to the substrate. The finished wafers were then scribed into 125 mil. square chips and bonded to TO-5 headers at 400°C. Gold wires were bonded to the aluminum contact pads and to the MOS guard-ring.

The phosphorus concentration in the substrate was obtained with good agreement from two standard methods: from the dependence of capacitance ($1/C^2$) on reverse voltage and from four-point probe measurements of the

starting resistivity. Values obtained by the capacitance method were then used because they are more accurate. By measurement of sheet resistance using a four-point probe, the boron surface concentration was found to be about 4×10^{19} cm^{-3}. The junction depth was determined by angle lapping and staining. The junctions are deep; for each base doping concentration, the emitter thickness x_j exceeds seven microns. This part of the design is meant to reduce the effects of band-edge distortion to secondary importance, as will be explained in Section 6.1.

Table I summarizes the physical make-up of the devices. The values of the Fermi level E_F given there are calculated from

$$E_F - E_I = kT/q \ln(N_{DD}/n_i)$$

using $n_i = 1.08 \times 10^{10}$ cm^{-3} at 297.5°K.

III. MEASUREMENT OF DEEP LEVELS IN THE BASE

To determine the extent to which the emitter influences the performance of the diodes just described, the contribution from the base must be understood and determined. The component of current coming from the base arises from the recombination of holes with electrons through deep-level recombination centers in the silicon energy gap. The properties of these centers are described by the following parameters: N_{TT}, the concentration of the centers, e_n and e_p, the electron and hole emission rates, c_n and c_p, the electron and hole capture rates. For low-level injection, recombination is characterized by the minority-carrier lifetimes, $\tau_{no} = 1/c_n N_{TT}$ for p-type material and $\tau_{po} = 1/c_p N_{TT}$ for n-type material. Various methods [4,5] exist for measuring the parameters, N_{TT}, e_n, e_p, c_n, and c_p, including their positional dependence.

TABLE I

Summary of Devices Studied

Device No.	Base doping $N_{DD}(cm^{-3})$	Junction depth x_j (μm)	E_F-E_I (297.5°K) (eV)
2-1-1p1	1.5×10^{14}	10.8	0.245
2-2-1p1	1.34×10^{15}	9.6	0.300
2-4-1p1	1.12×10^{16}	8.5	0.355
2-5-1p5	6.7×10^{16}	7.5	0.401

For our diodes, we studied the energy levels in the band gap by the capacitance-transient method [4,5]. Use of this method indicated that there are no levels in the lower half of the gap. In the upper half, the same four levels were observed, independent of the substrate phosphorous concentration. The thermal activation energies, E_C-E_T, and densities N_{TT} were determined to be as follows:

$E_C - E_T$ =	N_{TT} =
93 meV	3.3×10^{12} cm^{-3}
270 meV	4.3×10^{12} cm^{-3}
285 meV	2.0×10^{12} cm^{-3}
542 meV	3.5×10^{13} cm^{-3}

The thermal activation energies were obtained by fitting the experimental temperature dependencies of the thermal emission rates to the Arrhenius equation, as in Appendix A.

The electron thermal-emission rates for all four levels, determined by the transient capacitance method, are listed in Appendix A together with the hole thermal-emission rates for the midgap level, as calculated from the temperature dependence of the reverse-biased current [4].

The energy levels at 93 and 285 meV are probably due to the interstitial Mg double donor center [6], since the boron diffusion source contains MgO as one of its main constituents. The impurities responsible for the other two centers were not identified, but they also probably come from the binder impurities in the boron diffusion source. The midgap level at 542 meV has the largest density and will thus tend to dominate in determining the base recombination current. In all four devices, the density N_{TT} of each level listed above was approximately the same, within a factor of two. Measurements also indicated that N_{TT} was independent of position in the base.

Although it is a well-known procedure [4], we note again that the MOS guard-ring has to be a.c. grounded during capacitance transient measurements to avoid capacitance coupling between the p^+ and n regions through a floating MOS aluminum gate on the surface. Since the capacitance measurement is a three-terminal measurement, the MOS capacitance to ground is not recorded. Note also that levels in the lower half of the band gap will give a decreasing capacitance transient because $e_p^t > e_n^t$, which contrasts with the increasing capacitance transient due to the levels in the upper half of the band gap, which have $e_n^t > e_p^t$.

During measurements each device was mounted on a cold finger inserted in a liquid nitrogen dewar. Constant temperature was maintained by a temperature controller of a type designed by Sah and co-workers [7]. The temperature was calibrated to an accuracy of ±0.2°C, and the temperature change during the measurement was less than ±0.1°C.

IV. CURRENT-VOLTAGE CHARACTERIZATION

The determination of material parameters from measured data requires that the data be treated and the behavior of the device be described in ways that are consistent with the physics underlying device operation.

The physical mechanisms governing the operation of a forward-biased junction diode produce a current consisting of three components:

(a) A diffusion component due to the diffusion and recombination in the two quasi-neutral regions of the junction, as obtained by Shockley in the ideal diode theory [8], and extended by Moll and Ross [9] to include the effects of drift due to a built-in electric field.

(b) A recombination component due to carrier recombination in the bulk space-charge layer of the junction [10] and

(c) Surface components, including the surface channel current, the recombination current through bulk centers in the surface space-charge layer as well as through surface and interface states [11].

In silicon diodes, the recombination current in the bulk space-charge layer (component b above) dominates at small forward bias for room temperature or below while the diffusion current (component a above) dominates at medium bias levels [10]. Surface currents (components c above) obscure the properties of interest to this study, and the MOS guard-ring gate of the diode structure described in Section II provides a means to diminish and nearly eliminate their contributions. The magnitudes of the surface components depend on the surface potential, which can be controlled by applying a voltage to the MOS guard-ring gate electrode [11]. By adjusting this voltage to minimize the diode current, the influence of the surface components can be suppressed and in some devices made negligible compared with the bulk components (a) and (b) above.

The total diode current is the sum of all three components. The recombination and surface components (components b and c) can be combined into one term, $I_X = I_{XO}[\exp(qV/m_X kT) - 1]$, which is an empirical relationship that applies to the devices studied here. The total current is then the sum of two terms, given by

$$I = I_{XO}[\exp(qV/m_X kT) - 1] + I_{QNO}[\exp(qV/kT) - 1] \quad (1)$$

where I_{XO} and m_X are the coefficient and the reciprocal slope of the surface and bulk space-charge-layer components (components b and c).

In Eq. (1), the second term is the diffusion current (component a) for low-level-injection conditions. The coefficient I_{QNO}, which is customarily called the saturation current, consists of two parts, one from carrier recombination, diffusion and drift occurring in the quasi-neutral base and the other from these same processes occurring in the quasi-neutral emitter.

The expression for the diode current given in Eq. (1) correctly describes the physics underlying device behavior for low-level-injection conditions. Thus, as we shall see, experimental study of the saturation current I_{QNO} can help disclose the values of the material parameters of the quasi-neutral regions, including the values of the emitter and base lifetimes.

V. INCORRECT PROCEDURES FOR DETERMINING LIFETIME

Any characterization using an expression different from Eq. (1) is incorrectly linked to the underlying physics for low-level conditions and can lead to erroneous conclusions about the material parameters of the diode. As an example of such an erroneous link to the physics, consider the characterization [12,13]:

$$I = I_{01}(e^{qV/m_1kT} - 1) + I_{02}(e^{qV/m_2kT} - 1) , \qquad 1 \leq m_1 < m_2 \qquad (2)$$

The first term in this characterization is an empirical fit which has been regarded as related to the diffusion current (component a); in this empirical fit m_1 frequently is greater than 1. The second term is an empirical fit regarded as related to the bulk and surface space-charge-layer currents (components b and c). In some past work [14], the reciprocal slope m_2 has been set equal to 2, which corresponds to a special case of assumed properties of the recombination centers.

Equation (2) can describe the terminal characteristics of the single diode for which the empirical fit is made. But if this expression is used to calculate such material parameters as the base lifetime, it can yield values that differ by orders of magnitude from the actual values.

To illustrate this point, consider the forward-current characteristics shown in Fig. 1 for the diodes described in Section II. The characteristics were measured at a temperature of 297.5°K, and the surface component of the current was minimized by adjusting the voltage on the MOS guard-ring gate. The logarithmic dependence of current on voltage shows non-unity slope for all four types of diodes shown in Fig. 1. Most silicon diodes show a non-unity slope.

In an incorrect procedure of evaluation used by some authors [12,13], the diffusion current is approximated by the first term in Eq. (2). Then the saturation current I_{01} is the intercept on the ℓnI axis obtained by extrapolating the line of reciprocal slope m_1. The values of I_{01} resulting from this procedure, together with the reciprocal slope m_1, are listed in Table II. In the second step in the incorrect procedure, the current I_{01} is related to the material parameters by the Shockley ideal formula [8],

$$I_{01} = Aqn_i^2 \left[\frac{1}{N_{DD}} \sqrt{\frac{D_B}{\tau_{B01}}} + \frac{1}{N_{AA}} \sqrt{\frac{D_E}{\tau_{E01}}} \right] , \qquad (3)$$

where A is the device area, n_i is the intrinsic carrier concentration in silicon, N_{DD}, D_B, τ_B are doping density, diffusion coefficient and minority carrier lifetime, respectively, in the base, and N_{AA}, D_E, τ_E are the same parameters for the emitter region.

The incorrect procedure continues by assuming that only the base is important to the observed behavior, which gives

TABLE II

Summary of Material Parameters at 295.5°K

Device No.	A I_{01} (10^{-13} A)	B m_1	C $\tau_{B_{01}}$ (nsec)	D τ_m(JCR) (nsec)	E τ_m(OCVD) (nsec)	F τ_B (nsec)	G $\frac{\tau_B}{\tau_m(\text{OCVD})}$
2-1-1p1	500	1.11	4.3	255	325	330	≈1.0
2-2-1p1	52	1.09	3.8	150	115	120	≈1.0
2-4-1p1	11	1.14	0.9	90	115	120	≈1.0
2-5-1p5	4.6	1.15	0.08	40	105	145	1.4

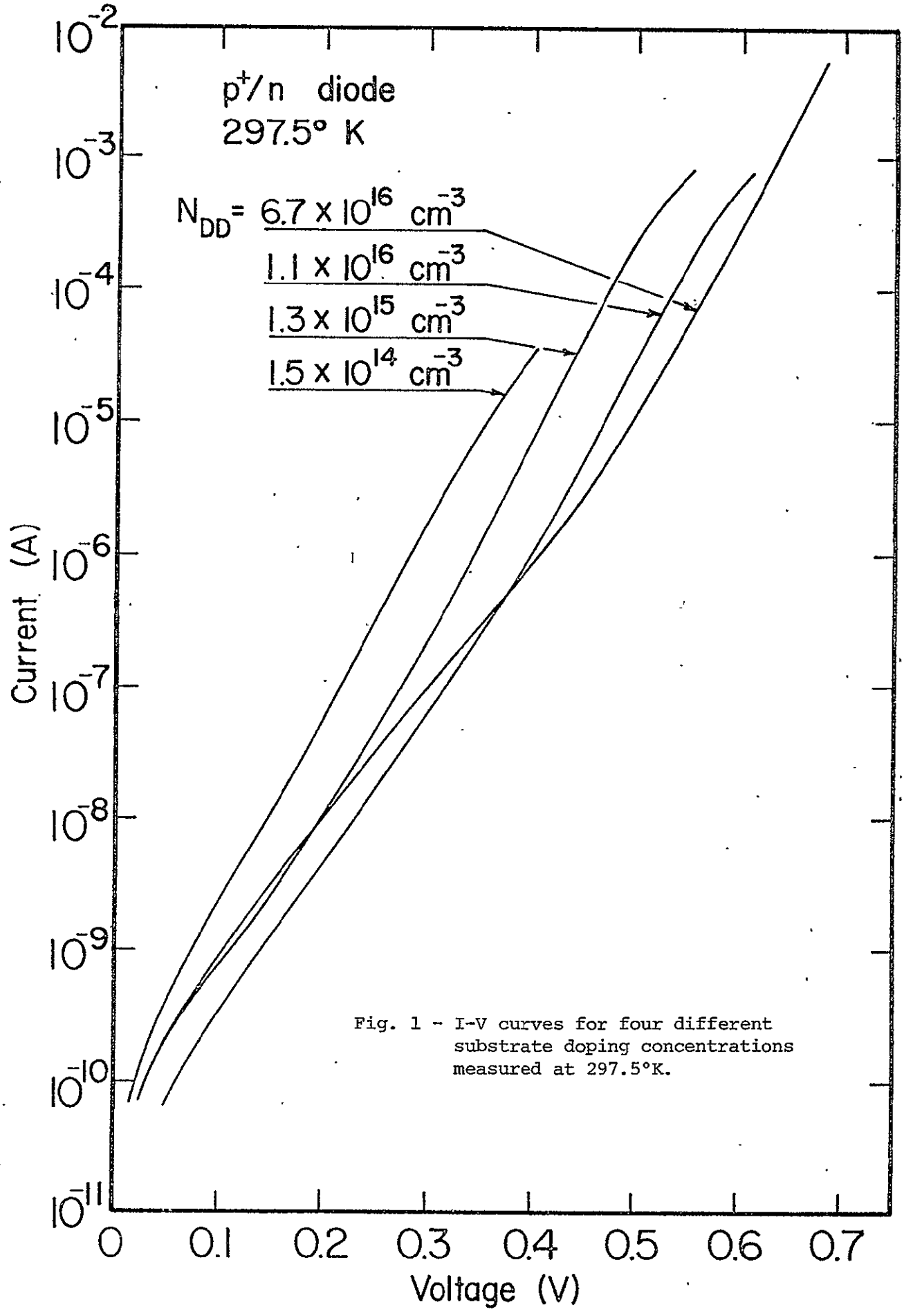

Fig. 1 - I-V curves for four different substrate doping concentrations measured at 297.5°K.

$$I_{01} = Aqn_i^2(1/N_{DD})\sqrt{D_B/\tau_{B01}} \qquad (4)$$

The incorrect base lifetime τ_{B01} is then solved from Eqn. (4) for each I_{01}, yielding the values in Table II listed in Column C as τ_{B01}. Note that the values deduced by this incorrect procedure are unreasonably small, especially for the more heavily doped devices. As will be seen shortly, the key to the correct procedure and the correct link to the physics lies in the realization that, in accord with Eq. (1), the line used to determine the saturation current must have unity slope. Extrapolation of this line will then give much larger values for the base lifetime τ_B than those listed in Column C of Table II. The correct procedure of requiring unity slope for the ideal Shockley component of current has been known for nearly twenty years.

A further discrepancy resulting from this incorrect procedure is disclosed by comparing the values of τ_{B01} in Table II, found from the I-V curve, with values of τ_B determined by more direct measurements of the lifetime. There are several standard methods of direct measurement of the base lifetime in p-n-junction diodes. The methods used most often are the junction-current-recovery (JCR) [15] and open-circuit-voltage-decay (OCVD) experiments [16]. For both methods, the conventional assumption is made that most of the excess charge resides in the base region, and, hence, the result τ_m of these measurements is generally assumed to give the effective base lifetime. In Table II, we compare τ_{B01} with τ_m(JCR) and τ_m(OCVD). Substantial disagreement exists. The smallest value of the ratio τ_m/τ_{B01} is about 30.

The incorrect procedure [12,13] just described is based on the following two assumptions:

(a) The saturation current I_{QNO} can be determined by extrapolating the measured dependence of ℓnI versus qV/kT using the empirical fit of Eq. (2), with slope $m_1 > 1$.

(b) The contribution to diode current from carrier recombination, drift and diffusion in the emitter is negligible compared with the contribution of these processes in the base.

Assumption (a) is incorrect for all p-n-junction diodes. It is not correctly based on the device physics. Assumption (b) is incorrect for diodes with heavily-doped bases. Its use can introduce sizable error in calculating the base lifetime and other device material parameters, as we shall see.

VI. CONTRIBUTION OF THE EMITTER REGION AND DETERMINATION OF BASE AND EMITTER LIFETIME

To determine the contribution of the emitter requires a model that includes the recombination, diffusion and drift processes which occur in the quasi-neutral emitter region. As Eq. (3) indicates, the original diode theory of Shockley [8] accounted for the recombination and diffusion of carriers in the emitter. But the Shockley model did not explicitly account for several mechanisms that may be present in modern silicon diodes. These mechanisms arise from various sources. For example [1]:

(a) the large electric field due to the gradient of the impurity concentrations produces minority-carrier drift as well as diffusion, which may be thought of as enhanced diffusion;

(b) the minority-carrier lifetime may depend on position, decreasing sharply in the direction toward the degenerately-doped emitter surface due to an increasing density of recombination centers toward the surface;

(c) the distortion of the energy band edges in the highly-doped material may also influence the spatial dependence of the carrier recombination rates in the emitter.

We now outline a simple lumped model [17] that is general enough to include all of these mechanisms, and discuss the use of this model in determining device material parameters, including the emitter and base lifetimes.

6.1 Model Including the Effect of the Emitter

As in Eq. (1), the current in a diode consists of components from the quasi-neutral emitter and base regions together with components coming from the bulk and surface space-charge regions. Using the principles of charge control [18], we rewrite Eq. (1) as

$$I = Q_E/\tau_E + Q_B/\tau_B + \sum (Q_{SC}/\tau_{SC}) \qquad (5)$$

in which Q_E and Q_B are the excess minority-carrier charges in the quasi-neutra emitter and base, $\sum Q_{SC}$ represents the effective excess mobile chargesof the bulk space-charge region and the surface region, and τ_E, τ_B, and τ_{SC} are the respective charge-control time constants or relaxation times. For time-varying conditions, the quasi-static approximation customarily used in charge-control analysis gives

$$i(t) = \frac{q_E}{\tau_E} + \frac{q_B}{\tau_B} + \frac{dq_E}{dt} + \frac{dq_B}{dt} + \sum\left[\frac{q_{SC}}{\tau_{SC}} + \frac{dq_{SC}}{dt}\right] \qquad (6)$$

for the diode current. To simplify the model, we neglect the last two components, which are bracketed in Eq. (6). As has been discussed, the surface currents can be suppressed by applying a voltage to an MOS guard-ring. The current from the bulk space-charge region and the remnants of the surface current not disposed of by the guard-ring can be removed from the experimental data by methods to be described.

If the diode current arises only from processes occurring in the quasi-neutral regions of the base and the emitter, then the expression for the static current given in Eq. (1) reduces to

$$I = I_{QNO}[\exp(qV/kT) - 1] , \tag{7}$$

and the excess minority carrier charges, Q_E and Q_B, in the quasi-neutral emitter and base depend on the diode voltage V according to

$$Q_E = Q_{EO}[\exp(qV/kT) - 1)], \quad Q_B = Q_{BO}[\exp(qV/kT) - 1)] \tag{8}$$

The validity of Eqs. (7) and (8) require the additional assumptions that no carrier high-injection levels occur in the quasi-neutral regions and that the effect of series resistance is negligible. These assumptions also necessitate care in treating the experimental data, which will be demonstrated shortly. The important point to be emphasized is that the relations given above in Eqs. (7) and (8) hold even in the presence of the various mechanisms listed earlier which may occur in modern silicon devices, including the effects of carrier drift, position-dependent lifetime, and band-edge distortion.

From Eqs. (5) through (8), we find that the saturation current I_{QNO} is given by

$$I_{QNO} = Q_{EO}/\tau_E + Q_{BO}/\tau_B , \tag{9}$$

and the relaxation time of the diode, including both the emitter and base regions, is given by [17]

$$\tau_m = (Q_{EO} + Q_{BO})/I_{QNO} . \tag{10}$$

The relaxation time τ_m characterizes the exponential response of the excess minority-carrier charges $q_E(t)$ and $q_B(t)$. If a steady forward current is applied and then removed, the excess minority charges $q_E(t)$ and $q_B(t)$ will decay or relax toward zero exponentially with time as $\exp(-t/\tau_m)$. The system of electrons and holes in the quasi-neutral regions relax toward the equilibrium state exponentially with time constant τ_m.

There are six unknowns in Eqs. (9) and (10): the relaxation time, the saturation current, the two effective lifetimes, and the two pre-exponential factors defined in Eq. (8). By methods to be described below, the relaxation time and the saturation current can be determined from experimental data. If values can be fixed for any two of the remaining unknowns, then all six unknowns are determined. In general this may require experiments [19] in addition to those described in this paper, as well as computer solutions [20] of the differential equations underlying the diode characteristics. But, for the diode structures studied here, the design justifies additional approximations that immediately determine Q_{EO} and Q_{BO}, simplifying the problem greatly.

To determine Q_{EO}, we note that the junctions are deep. Thus the carriers injected into the quasi-neutral emitter never reach the highly-doped part of the emitter, and the effects of band-edge distortion can be neglected. Hence, using this assumption together with the assumption

of an exponential doping profile in the emitter, one can show that [21]

$$Q_{EO} \simeq (Aqn_i^2/N_{AA}) W_E/\ell n(P_{MAX}/N_{AA}) \quad . \tag{11}$$

This implies that the electric field due to the gradient of impurity concentration, in effect, packs the carriers into a thin region near the junction space-charge region. For example, if $P_{MAX}/N_{AA} \simeq 10^4$, this thin region occupies about one-tenth of the thickness W_E of the quasi-neutral emitter. Here N_{AA} denotes the doping concentration at the emitter edge of the junction space-charge region and P_{MAX} is the majority carrier concentration at the emitter surface. To a first approximation, which neglects the de-ionization of impurity atoms in heavily-doped material, P_{MAX} equals approximately the surface impurity concentration. A suitable value of N_{AA} to be substituted into Eq. (11) can be found from a linearly-graded model of the junction [22].

To determine Q_{BO} for the diodes under study, we use the observation noted in Section III that the densities of the deep energy levels in the base show no spatial dependence. This permits the use of the widely-known approximation,

$$Q_{BO} \simeq (Aqn_i^2/N_{DD}) \sqrt{D_B \tau_B} \tag{12}$$

in which N_{DD} is the impurity concentration of the homogeneous base. The value of N_{DD} can be found from measuring the dependence of small-signal capacitance on reverse bias, a method that is commonly used.

Hence, for the diode structures designed for this study, determination of the contribution of the emitter to the diode characteristics, and of the emitter and base lifetimes, requires only that I_{QNO} and τ_m be experimentally determined and then combined with Eqs. (9) through (12).

6.2 Determination of the Saturation Current I_{QNO}

The parameter I_{QNO} in the model above corresponds to the diffusion component (component a) of the diode current described in Section IV. Summing this component with the component representing the bulk and surface space-charge layers, as in Eq. (1), yields the total diode current. The first step in determining I_{QNO}, therefore, is to separate the measured static I-V dependence into the two components of Eq. (1). This involves subtracting the bulk and surface component, which has a reciprocal slope $m_x > 1$, from the measured diode current to reveal the diffusion component, which has a reciprocal slope m=1. The procedure is shown in Fig. 2. In this figure, the broken line is the extrapolated bulk and surface component. The solid curve is the measured I-V dependence. Subtraction yields the line that passes through the dots, which is the ideal diffusion component of the diode current and has a reciprocal slope m=1. The ideal diffusion component can dominate in determining the measured current over a considerable range of current. For the example of Fig. 2, the range is about two decades of current. At higher currents, the measured current may drop below the ideal component, with m > 1, either because of series resistance or high injection or both.

By the procedure shown in Fig. 2 the saturation current I_{QNO} is thus simply and unambiguously given by the intersection of the ideal diffusion component with the V=0 axis. For the diodes studied here, the results thus derived for I_{QNO} are shown in the first column of Table III.

An alternate method exists to determine I_{QNO}. This simply involves taking the I-V measurement at higher temperatures, which emphasizes the

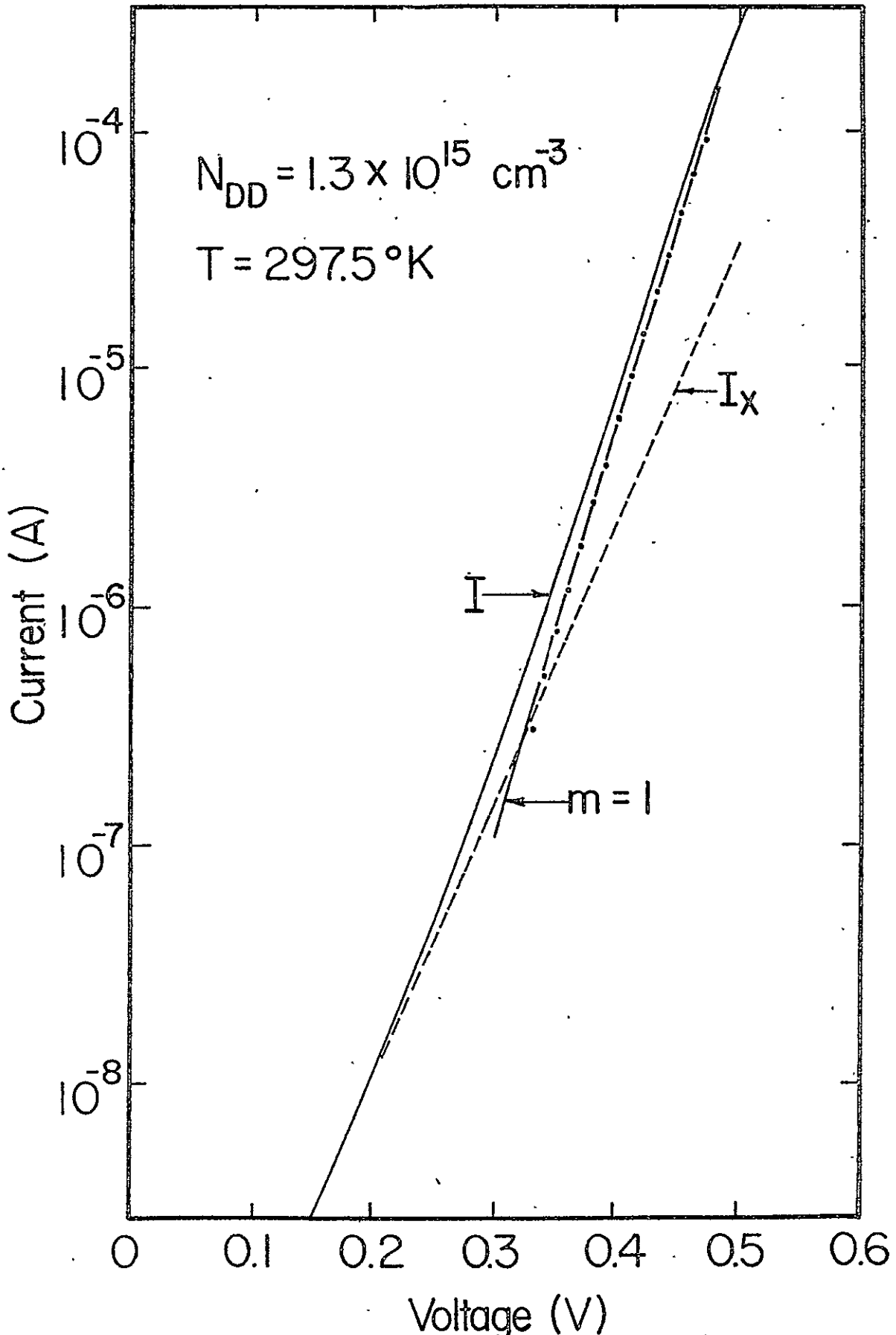

Fig. 2 - Separation of the I-V curve into components. The solid curve is the measured I-V dependence. The broken line is extrapolated bulk and surface component. Ideal diffusion component passes through the dots.

dominance of the diffusion component. At a high enough temperature, the reciprocal slope becomes essentially unity over several decades of current, enabling direct extrapolation of the measured current to V=0 without the necessity of subtracting and decomposing into components. For diodes having reciprocal slopes within about ten percent of unity at room temperature, we found that increasing temperature by 30°C sufficed to produce unity slope.

An additional test can be made to determine the voltage range over which the diffusion component dominates and thus to lend further confidence to the procedure by which I_{QNO} is determined. This test involves measuring the dependence of forward current on temperature, which gives the activation energy. If the diffusion component dominates at the forward voltage under study, theory [8] predicts that the activation energy will be approximately the band gap. If not, it will be about one-half of the band gap. This measurement was made for several diodes at voltages in the middle of the voltage range for which the diffusion component appeared to dominate. The result deduced from this measurement was about 1.1 eV, which is in close agreement with the value of the silicon energy gap.

6.3 Determination of the Relaxation Time

In general, the relaxation time, τ_m, can be found by measuring the diode response to some form of time-varying excitation. Of the several methods available to determine the relaxation time this way, we used two: the junction-current-recovery (JCR) method [15] and the open-circuit-voltage-decay (OCVD) method [16].

As the preceding discussion in this section has emphasized, whatever method is used we must confine the measurement to that range of

voltages for which the diffusion component of the diode current dominates over the component coming from recombination in the surface and bulk space-charge layers. In this regard, OCVD has the advantage. Fig. 3 illustrates a typical OCVD response. After an initial jump due to the cessation of current through the series resistance, the response shows a linear variation in time, having a slope, dV/dt.

The voltage range of this constant slope corresponds to the range seen on the static I-V characteristics for which the diffusion component dominates. Thus if we assume $\left|\frac{dq_{SC}}{dt}\right| << \left|\frac{dq_E}{dt} + \frac{dq_B}{dt}\right|$ in Eq. (6), then

$$\tau_m = -\frac{kT}{q}\frac{1}{dV/dt}, \tag{13}$$

which is the relaxation time constant describing the quasi-neutral regions. As the voltage decreases beyond this range, Fig. 3 illustrates that the slope lessens, a result of the increasing role of the recombination component from the bulk and surface space-charge layers. But, by focusing on the initial portion of the response and using Eq. (13), one can find the relaxation time which is dominated by the charges stored in the quasi-neutral emitter and base regions. This is the relaxation time of the model described in Section 6.1.

In contrast, determination of τ_m by JCR involves some average over a range of forward voltage that includes a low-current range where the diffusion component is insignificant while the components from the bulk and surface space-charge-layers dominate.

We used both OCVD and JCR to determine τ_m, keeping the maximum forward voltage applied to the diode below that which would cause high injection. Results obtained by both methods are compared in Table II.

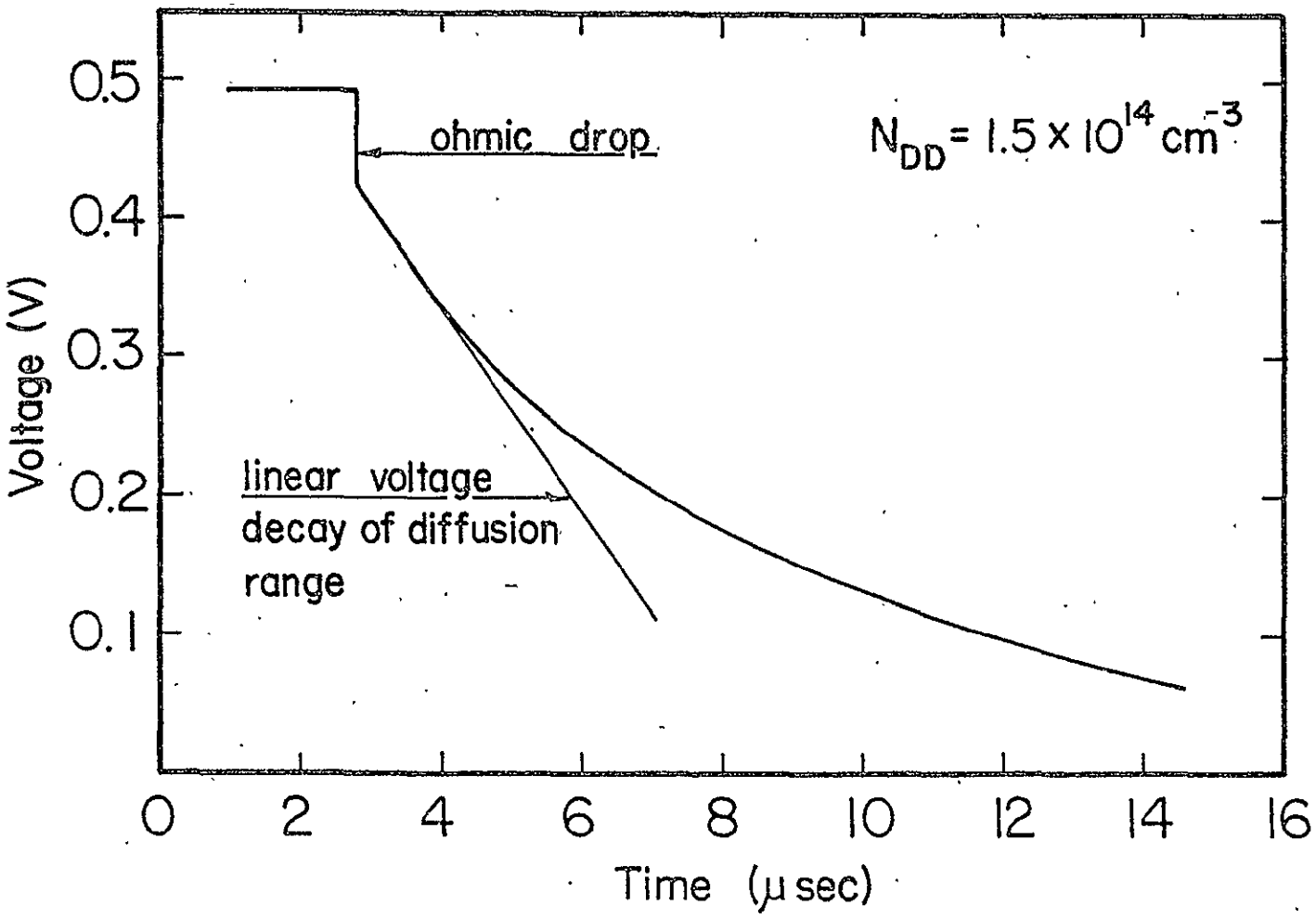

Fig. 3 - Typical OCVD response showing the distinctive linear decay in the diffusion range.

In all discussions to follow in this paper, the values used will be those found from the OCVD method, which are the more appropriate values for the reasons just stated.

As was noted in Sec. 6.2, raising the temperature increases the dominance of the diffusion component. Thus, in the OCVD response, an increase in temperature extends the voltage range for which the initial constant slope prevails. This was done for several diodes, and the values of the lifetimes were calculated. These lifetimes agreed with those determined at room temperature. The results of this procedure justifies the neglect of the bracketed components in Eq. (6).

A variation of the OCVD method could be used which restricts the response itself to the range for which the diffusion component is dominant. In this variation, the diode is biased in this range and then a small pulse of current is superimposed. The voltage response is linear with time, showing a single slope.

Apart from the JCR and OCVD methods, τ_m can also be obtained from measuring immittance of the diode versus frequency [20,22,23].

6.4 Emitter and Base Lifetimes and Other Material Parameters

Combining I_{QNO} and τ_m, as determined by the experiments described in the preceding sections, and using the theoretical relations described in these sections, we obtain the effective emitter and base lifetimes, τ_E and τ_B. In Tables II and III these are listed for each of the four substrate doping concentrations being studied. These tables contain also the pre-exponential factors Q_{EO} and Q_{BO} in Eq. (8) which give the charges of the excess minority carriers, Q_E in the emitter and Q_B in the base. To emphasize the contribution of the emitter to the diode characteristics, various ratios involving these material parameters are displayed in Tables II and III.

TABLE III

Summary of Material Parameters at 297.5°K

Device No.	A I_{QNO} (10^{-13} A)	B Q_{EO} (10^{-22} C)	C Q_{BO} (10^{-20} C)	D τ_E (nsec)	E $\frac{Q_{EO}/\tau_E}{Q_{BO}/\tau_B}$ (%)	F Q_{EO}/Q_{BO} (%)	G $\frac{Q_{EO}/\tau_E}{I_{QNO}}$ (%)	H $\frac{\tau_E}{\tau_B}$
2-1-1p1	55	610	170	235	5	4	5	0.7
2-2-1p1	10.2	76	11	95	9	7	8	0.8
2-4-1p1	1.1	13	1.15	90	15	11	13	0.8
2-5-1p5	0.18	3	0.16	40	65	19	40	0.3

VII. DISCUSSION

The emitter has more influence on the characteristics of the diodes having the higher substrate impurity concentrations, which is to be expected on qualitative grounds. With regard to the static characteristics, Column G of Table III exhibits how the emitter contribution to the total current depends on the substrate concentration. This emitter contribution reaches about 40% of the total current for device 2-5-1p5 ($N_{DD} = 6.7 \times 10^{16}$ cm^{-3}). As column E of Table III shows, this corresponds to an emitter current that is about 65% of the base current. This emitter contribution for device 2-5-1p5 is more accurately determined than the contributions for the diodes having lower substrate concentrations. For these devices, the figures listed for the emitter contributions are less accurately determined because their calculation involves subtracting two nearly equal numbers.

With regards to the transient characteristics, Column G of Table II demonstrates that the base lifetime does not necessarily equal the time constant measured by open-circuit-voltage decay. For device 2-5-1p5, an error of about forty percent in the calculated base lifetime is introduced if the emitter contribution to the transient response is neglected.

lifetime is considerably lower than the base lifetime in the device (2-5-1p5) with the highest substrate doping and the shallowest junction. For this device, recombination within the emitter occurs in a region of relatively high doping that is relatively close to the degenerately-doped surface.

The results discussed above apply to the particular diodes fabricated for this study. They demonstrate quantitatively the importance of recombination in the emitter to both the static and transient characteristics. This demonstration was one purpose of this paper. But the main emphasis of the paper is on the method which yields the results. For the first time, a method is described which separates as well as determines the emitter and base lifetimes in a p-n-junction device after the junction has been fabricated.

The method involves the following measurements: (i) the static current-voltage dependence, (ii) the transient open-circuit-voltage decay, (iii) the capacitance versus reverse voltage, and (iv) the thermally-stimulated, voltage-stimulated and light-stimulated capacitances [4,5]. These methods of measurement are not new. The novelty presented here lies in combining and interpreting the results of these various measurements with simple models that are consistent with the physics underlying the electrical characteristics of semiconductor p-n-junction diodes. A major result is that the method presented here discloses the base and emitter lifetimes concealed in the experimental data.

The design of the diodes used here has permitted the study of the emitter and base lifetimes unobscured by the possible effects of energy band-edge distortion (gap shrinkage) which may be present in the emitter.

The diodes were designed to have deep junctions with moderate impurity gradients on silicon substrates having impurity concentrations not exceeding 10^{17} atoms/cm^3. This allows us to calculate the equilibrium emitter charge Q_{EO} defined in Eq. (8) under the assumption of no energy gap shrinkage in the thin portion of the quasi-neutral emitter where many minority electrons exist.

The self consistency of this assumption can be easily demonstrated for the diodes studied. From the assumption of negligible gap shrinkage it follows that the excess carriers within the emitter are packed by the built-in electric field into a thin region adjoining the junction space-charge region. In Section 6.1, we noted that this active portion of the quasi-neutral emitter extends from approximately $x = x_1 = W_E\{1 - \frac{1}{\ell n[P_{MAX}/N_{AA}(W_E)]}\}$ to $x = W_E$. Hence, the assumption of negligible gap shrinkage is self-consistent if $N_{AA}(x_1)$ is sufficiently small. The assumption is most questionable for the diode (2-5-1p5) having the highest base doping concentration and the shallowest junction. For this device, using a gaussian approximation of the doping profile, we calculate that $N_{AA}(x_1)$ is about 2×10^{17} atoms/cm^3. At this impurity concentration, little gap shrinkage can occur [25], which demonstrates the self consistency of the assumption.

But this assumption is questionable for p-n-junction devices having shallower junctions, and higher impurity gradients and base doping concentrations. For such devices, besides the emitter and base lifetimes, the energy gap shrinkage in the emitter needs to be determined. Variations of the method described here, involving additional measurements, have been used to determine the energy-gap shrinkage for p-n-junction solar cells and for p-n-junction transistors [26]. In Chapter 4, we describe the application of these methods to n-on-p solar cells.

APPENDIX A (of CHAPTER II)

Electron thermal-emission rates from transient-capacitance measurements for four imperfection levels in the upper half of the bandgap are:

$$e_n^t = (7.7\pm2.1)10^4(T/300)^2\exp(-93\pm2)/k_BT \text{ sec}^{-1}$$

$$e_n^t = (1.51\pm1.1)10^{11}(T/300)^2\exp(-270\pm7.4)/k_BT \text{ sec}^{-1}$$

$$e_n^t = (8.72\pm4.5)10^{10}(T/300)^2\exp(-285\pm6.4)/k_BT \text{ sec}^{-1}$$

$$e_n^t = (2.89\pm1.3)10^{11}(T/300)^2\exp(-542\pm8.6)/k_BT \text{ sec}^{-1}$$

The hole thermal-emission rate for the midgap level, obtained from measurement of diode reverse leakage current [4], is given by

$$e_p^t = (1.2\pm0.46)10^9\ (T/300)^2\exp(-593\pm9.5)/k_BT \text{ sec}^{-1}.$$

REFERENCES FOR CHAPTER 3

1. F.A. Lindholm and C.T. Sah, "Fundamental Electronic Mechanisms Limiting the Performance of Solar Cells," IEEE Trans. Electron Devices, April1977.

2. C.T. Sah and C.T. Wang, "Experiments on the Origin of Process Induced Recombination Centers in Silicon," J. Appl. Phys., vol. 46, pp. 1767-1776, April 1975.

3. L.D. Yau and C.T. Sah, "Quenched-in Centers in Silicon p^+n Junctions," Solid-State Electronics, vol. 17, pp. 193-201, Feb. 1974.

4. C.T. Sah, L. Forbes, L.L. Rosier and A.F. Tasch, Jr.," Solid-State Electronics, vol. 13, pp. 759-788, June 1970. See also a review treating these and more recent methods in C.T. Sah, "Bulk and Interface Imperfections in Semiconductors," Solid-State Electronics, vol. 19, pp. 975-990, Dec. 1976.

5. C.T. Sah, "Detection of Recombination Centers in Solar Cells from Junction Capacitance Transients," IEEE Trans. Electron Devices, April 1977.

6. L.T. Ho and A.K. Ramdas, "Excitation Spectra and Piezospectroscopic Effects of Magnesium Donors in Silicon, Physical Review B, vol. 5, pp. 462-474, Jan. 1972.

   S.T. Pantelides and C.T. Sah, "Theory of Localized States in Semiconductors. II. The Pseudo Impurity Theory Application to Shallow and Deep Donors in Silicon," Physical Review B, vol. 10, pp. 638-658, July 1974.

7. C.T. Sah, L.L. Rosier and L. Forbes, "Low-Temperature High-Frequency Capacitance Measurements of Deep- and Shallow-Level Impurity Center Concentrations," Appl. Phys. Letts., vol. 15, pp. 316-318, Nov. 1969.

8. W. Shockley, "The Theory of p-n Junctions in Semiconductors and p-n Junction Transistors," Bell Sys. Tech. J., vol. 28, pp. 435-489, July 1949.

9. J.L. Moll and J.M. Ross, "The Dependence of Transistor Parameters on the Distribution of Base Layer Resistivity," Proc. IRE, vol. 44, pp. 72-80, Jan. 1956.

10. C.T. Sah, R.N. Noyce, and W. Shockley, "Carrier Generation and Recombination in p-n Junctions and p-n Junction Characteristics," Proc. IRE, vol. 45, pp. 1228-1243, Sept. 1957.

11. C.T. Sah, "Effect of Surface Recombination and Channel on p-n Junction and Transistor Characteristics," IRE Trans. on Electron Devices, vol. ED-9, pp. 94-108, Jan. 1962.

12. R.J. Stirn, "Junction Characteristics of Silicon Solar Cells," Record of 9th Photoltaic Specialists Conference, pp. 72-82, 1972.

13. G.F. Wakefield, P.D. Maycock, and T.L. Chu, Record of 11th Photovoltaic Specialists Conference, pp. 49-55, 1975.

14. R.J. Stirn, "Role of Recombination Current on Photovoltaic Parameters," Chapter 17 in High Efficiency Silicon Solar Cell Review, NASA TM X-3326, pp. 157-165, Dec. 1975.

15. R.H. Kingston, "Switching Time in Junction Diodes and Junction Transistors," Proc. IRE, vol. 42, pp. 829-834, May 1954.

H.J. Kuno, "Analysis and Characterization of p-n Junction Diode Switching," IEEE Trans. on Electron Devices, vol. ED-11, pp. 8-14, Jan. 1964.

16. S.R. Lederhandler and L.J. Giacoletto, "Measurement of Minority Carrier Lifetime and Surface Effects in Junction Devices," Proc. IRE, vol. 43, pp. 477-483, April 1955.

17. F.A. Lindholm and C.T. Sah, "Normal Modes of Semiconductor pn Junction Devices for Material-Parameter Determination," J. Appl. Phys., vol. 47, pp. 4203-4205, Sept. 1976.

18. E.O. Johnson and A. Rose, "Simple General Analysis of Amplifier Devices with Emitter, Control, and Collector Functions," Proc. IRE, vol. 47, pp. 407-418, March 1959.

R.D. Middlebrook, "A Modern Approach to Semiconductor and Vacuum Device Theory," IEEE Proc., vol. 106B, suppl. 17, pp. 887-902, March 1960.

P.E. Gray, D. DeWitt, A.R. Boothroyd, and J.F. Gibbons, Physical Electronic and Circuit Models of Transistors, Wiley, New York, 1964.

19. F.A. Lindholm, A. Neugroschel, C.T. Sah, M.P. Godlewski, and H.W. Brandhorst, Jr., "Methodology for the Experimental Determination of Gap Shrinkage and Lifetimes in the Emitter and Base of pn-Junction Diodes and Solar Cells," IEEE Trans. Electron Devices, April 1977; also paper 1.1, Record of Twelfth Photovoltaic Specialists Conf., Nov. 1976.

20. H. Maes and C.T. Sah, "Application of the Equivalent-Circuit Model for Semiconductors to the Study of Au-doped p-n Junctions under Forward Bias," IEEE Trans. on Electron Devices, vol. ED-23, pp. 1131-1143, Oct. 1976.

21. F.A. Lindholm, "Simple Expressions for the Minority-Carrier Charge in the Emitter of p-n-Junction Devices," to be published.

22. C.T. Sah, "Effects of Electrons and Holes on the Transition Layer Characteristics of Linearly Graded p-n Junction," Proc. IRE, vol. 49, pp. 603-618, March 1961.

23. W. Shockley, Electrons and Holes in Semiconductors, pp. 313-318, Van Nostrand, Co., N.Y., 1950.

24. F.A. Lindholm, A. Neugroschel, and C.T. Sah, "Junction Modeling for Solar Cells Theory and Experiment," Technical Digest 1976 Int. Electron Devices Meeting, Washington, pp. 61-64, Dec. 1976.

25. D.D. Kleppinger and F.A. Lindholm, "Impurity Concentration Dependent Density of States and Resulting Fermi Level for Silicon," Solid State Electronics, vol. 14, pp. 199-207, 1971.

26. A. Neugroschel, F.A. Lindholm, and C.T. Sah, "Experimental Determination of Emitter Lifetime and Band-Edge Distortion in Transistors," to be published.

CHAPTER IV.
METHODS FOR DETERMINING THE EFFECTIVE GAP SHRINKAGE (MINORITY-CARRIER STORAGE) AND EFFECTIVE LIFETIME IN THE EMITTER

I. INTRODUCTION

The electrical characteristics of p-n-junction solar cells depend upon the recombination, generation, and transport properties of the mobile electrons and holes within the device material. These properties were first described by Shockley [1] in his ideal diode theory, which treated the relevant material parameters as constants. But within the emitter of a modern silicon cell the behavior of these properties can be more complex than that assumed in the ideal diode theory because of the presence of band-edge distortion (energy-gap shrinkage) and of position-dependent recombination rates [2]. As was discussed in Chapters I and II, these two mechanisms have been suggested as probable reasons for certain discrepancies between the theoretical and experimental performance, particularly the discrepancy of 100 millivolts in the open-circuit voltage seen in diffused-emitter silicon solar cells made with low-resistivity substrates [3]. Previously the physical mechanisms occurring in the emitter have been the subject of speculation and theoretical studies; no means has been available to investigate and characterize these mechanisms by experiment.

This chapter describes an experimentally-based methodology for determining the effective lifetime and the effective gap shrinkage (minority-carrier storage) in the emitter of p-n-junction solar cells. The methodology pertains to a solar-cell structure after the junction has been fabricated. Its use distinguishes the emitter region from the base region, yielding material parameters that apply to each of these two regions. Thus it enables a determination of the relative roles of the emitter and base in governing solar-cell performance, and an assessment of the importance of gap shrinkage relative to that of large recombination rates in the highly-doped emitter.

This chapter will emphasize the methodology--that is, the strategy of the procedures used and the physical principles underlying them. In the organization of the chapter, some of the theoretical grounds for the methodology are first described. This leads naturally then to the experimental measurements used and the physical interpretation of the data. To illustrate the procedures, they are applied to an n^+-p-junction solar cell having a substrate resistivity of about 0.1 ohm-cm.

II. A MODEL RELATING STATIC AND DYNAMIC RESPONSE

To provide a basis for studying the material parameters of the emitter and the base, a model of diode behavior is needed that is general enough to apply:

(a) in the presence of high, position-dependent recombination rates and of gap shrinkage;

(b) for any doping profile associated with the p-n-junction.

Recently such a model was proposed [4]. This model was outlined in Chapter III but we sketch its development here again to emphasize certain of its features that bear on the methodology and to enable this chapter to be read independently of Chapter III.

As is discussed in Chapter I and in the Appendix, an understanding of cell behavior in the dark is of central importance to the discrepancy between theoretical and experimental values of V_{OC} seen in low-resistivity silicon cells. Thus, consider a p-n-junction diode in the dark. In the ideal model of Shockley, the diode is divided into two types or regions:

(a) the quasi-neutral emitter and base; and

(b) the junction space-charge or transition region.

In a practical silicon diode, other space-charge regions may also exist, at the oxide-silicon interface and at the current contacts [5].

We now write the static (or d.c.) current, I, as the components from the quasi-neutral emitter and base regions added to the components coming from the bulk and surface space-charge regions. By the principles of charge control [6],

$$I = Q_E/\tau_E + Q_B/\tau_B + \sum [Q_{SC}/\tau_{SC}] \ . \qquad (1)$$

Here Q_E and Q_B designate the magnitude of the charge of the excess minority carriers in the quasi-neutral emitter and base, and ΣQ_{SC} denotes the effective moble charges stored in the bulk and the surface space-charge regions. The parameters τ_E, τ_B, and τ_{SC} are the relevant charge-control time constants or relaxation times.

To describe the current i(t) under dynamic conditions, we write

$$i(t) = \frac{q_E}{\tau_E} + \frac{q_B}{\tau_B} + \frac{dq_E}{dt} + \frac{dq_B}{dt} + \sum \left[\frac{q_{SC}}{\tau_{SC}} + \frac{dq_{SC}}{dt} \right] , \qquad (2)$$

which follows from the quasi-static approximation used in charge-control analysis [6]. In Eqs. (1) and (2), the components of current from the space-charge regions are bracketed for emphasis.

The methodology presented in this paper will emphasize the material parameters describing the quasi-neutral emitter and base. Hence the components of the current arising from the space-charge regions will be neglected in Eqs. (1) and (2). This approximation simplifies the model. But it requires that care be taken in experimental measurements; either conditions must be designed to make these space-charge-region components negligible or they must be removed from the experimental data to reveal the behavior coming from the quasi-neutral regions. In Sections III and

IV of this paper, we will describe specific procedures for dealing with the space-charge-region components and for dealing with other assumptions to be made in developing the model for diode behavior.

If this approximation is combined with the assumptions of low injection and negligible series resistance, the currents and the excess charges can be written simply:

$$i = I_{QNO}[\exp(qv/kT) - 1] \tag{3}$$

$$q_E = Q_{EO}\exp[(qv/kT) - 1];\ Q_{BO}\exp[(qv/kT) - 1] \tag{4}$$

Here $v = v(t)$ designates the total time-dependent voltage at the terminals of the diode. The subscript QN emphasizes that the saturation current I_{QNO} derives from processes occurring within the quasi-neutral regions. The additional assumptions needed to yield Eqs. (3) and (4) also require special care, to be discussed, in the design of experiments and in the interpretation of the data.

Combining Eqs. (1) through (4) gives

$$I_{QNO} = Q_{EO}/\tau_E + Q_{BO}/\tau_B \tag{5}$$

for the saturation current. By setting $i(t) = 0$ in (2) and solving the resultant differential equation, we find [4]

$$\tau_{QN} = (Q_{EO} + Q_{BO})/I_{QNO} \tag{6}$$

for the relaxation time of the model. This relaxation time determines the natural (force-free) behavior after the device is perburbed by an applied force, such as by an impulse current or a voltage step. It is an important parameter in determining the response of the diode to any time-varying (current) driving force.

Although simple, Eqs. (5) and (6), prove to be powerful relations for determining parameters of the quasi-neutral material. As will be

seen, the charge Q_{EO} is closely related to gap shrinkage occurring in the emitter; and τ_E is the effective lifetime of the minority carriers in the emitter, which relates to the position-dependent recombination rates that may be present there. Hence, it becomes of interest to see how Q_{EO} and τ_E--and their counterparts for the base Q_{BO} and τ_B--can be determined from experimental data.

The possibility of doing this depends on which of the six unknowns appearing in Eqs. (5) and (6) can be measured and which can be calculated by auxiliary relations. There are many possible measurements that apply to this problem, and some of these will be discussed in Section III. The measurements discussed in Section III will pertain to the determination of I_{QNO}, τ_{QN}, Q_{BO}, and τ_B.

Theory offers, in addition, certain auxiliary relations. First, if the minority-carrier lifetime and the net doping concentration both stay constant with position in the base, then from the conventional theory for low injection, we have for the base region,

$$Q_{BO} = qn_i^2 L_n / N_{AA} \ , \tag{7}$$

where $L_n = \sqrt{D_n \tau_n}$ is the minority-carrier diffusion length in the base, n_i is the intrinsic carrier concentration, and N_{AA} is the doping impurity concentration in the base for the n^+-p structure treated here. The spatial constancy of N_{AA} and τ_n can be assessed by the capacitance and transient-capacitance measurements indicated in Section III.

Besides Eq. (7), there is a second theoretical relation of interest. Let Q_{EO}^O designate the charge Q_{EO} <u>in the absence of gap shrinkage</u> in the emitter. By a simple extension of conventional theory, a relation for Q_{EO}^O can be found [7]. Fig. 1 illustrates the physics underlying this

relation. The gradient of the impurity concentration in the emitter produces a built-in electric field that packs the injected minority carriers into a thin region near the edge of the junction space-charge region. Integrating the density P(x) of the minority holes yields [7]

$$Q_{EO}^{O} = \left[qn_i^2/N(W_E)\right] \left\{ \frac{W_E}{\ell n[N_{MAX}/N(W_E)]} \right\} \tag{8}$$

in which N_{MAX} is the maximum majority-carrier concentration and $N(W_E)$ is the majority-carrier concentration at the emitter edge of the junction space-charge region. From Eq. (8), to a first approximation, the minority carriers can be viewed as restricted to the region, $W_E \left[1 - \frac{1}{\ell n \left[\frac{N_{MAX}}{N(W_E)}\right]}\right] < x < W_E$, which can be regarded as the active portion of the emitter of the dark diode in the absence of gap shrinkage. This point of view is emphasized by the dashed rectangle drawn in Fig. 1.

In eq. (8), $x = W_E$ corresponds to the emitter edge of the junction space-charge region. If the doping profile is assumed to be distributed spatially as any monotonically decreasing function, such as a Gaussian or an exponential function, then W_E will also be the thickness of the quasi-neutral emitter and N_{MAX} will be the majority-carrier concentration at the surface. But if the profile is practically flat over part of the quasi-neutral emitter, then W_E will stand for the distance from the edge of the junction space-charge region to the plane where the doping concentration starts to rapidly decline. To get an accurate estimate of Q_{EO}^{O}, an accurate estimate of the built-in electric field near the junction space-charge region is required. The meaning of W_E just discussed helps provide this estimate. It applies unless the doping concentration is practically flat over the entire quasi-neutral emitter, in which case the built-in electric field is nearly zero and Eq. (8) is invalid.

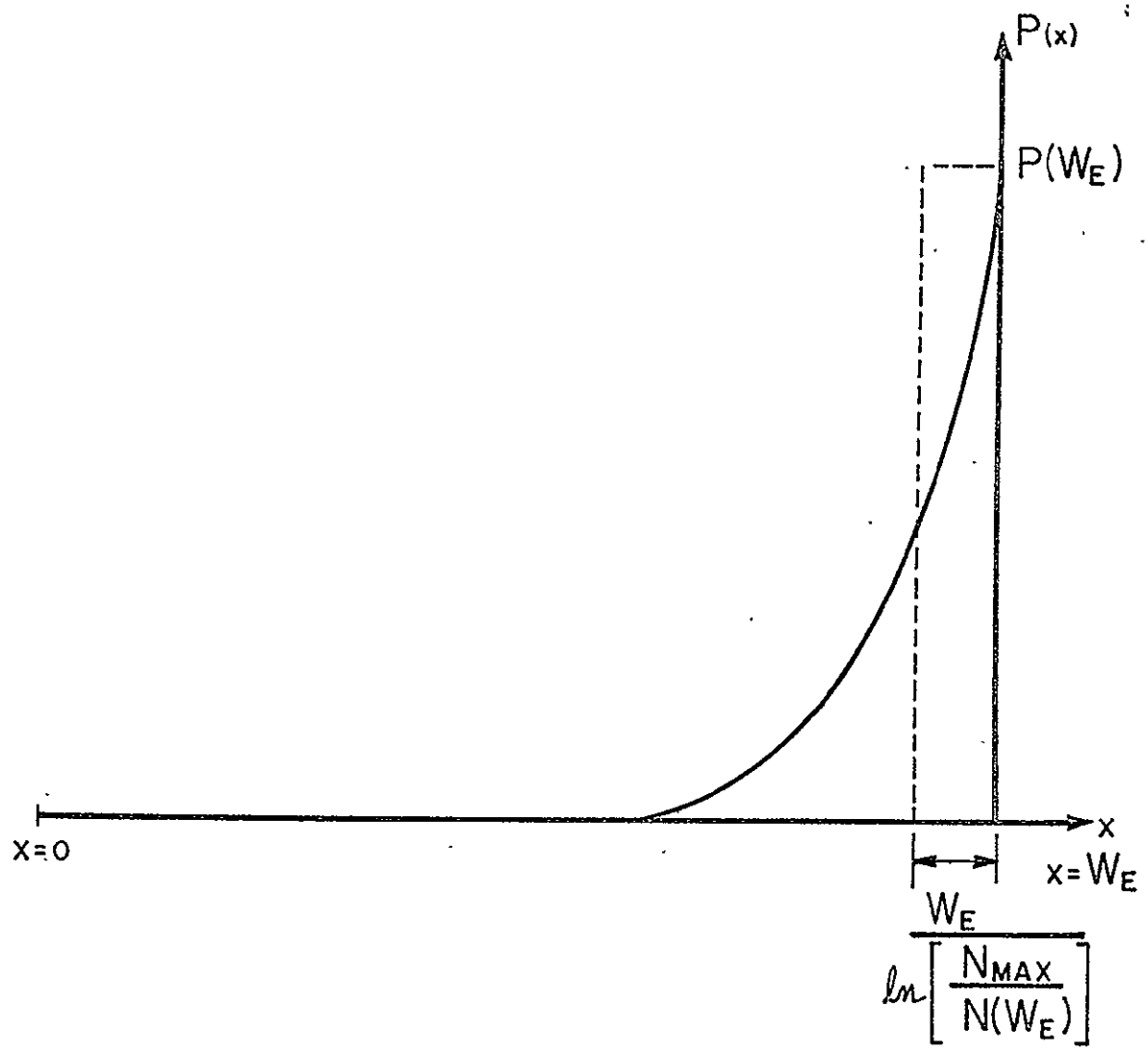

Fig. 1 The distribution P(x) of the excess minority carriers (holes) in the quasi-neutral emitter of a dark solar cell. The surface is at x = 0 and the edge of the junction space-charge region is at $x = W_E$. The area of the dashed rectangle equals the area under the curve, P(x).

Equation (8), defining Q_{EO}^{o}, has several uses. First, it permits an approximate calculation of the emitter doping density at $x = W_E\left[1 - \frac{1}{\ell n[N_{MAX}/\bar{N}(W_E)]}\right]$, which is the maximum density in the active portion of the emitter. If this density falls below about 10^{18} atoms/cm^3, the gap shrinkage in the active portion is negligible [8]. Hence, as a trial calculation, the gap shrinkage can be assumed to be negligible and Q_{EO} can be calculated from Eq. (8). This assumption can then immediately be tested for self-consistency, in the manner just described. For devices having junctions deep enough as well as small enough impurity gradients and base doping concentrations, this assumption will be self-consistent. Thus Q_{EO} calculated from Eq. (8) can be combined with Eqs. (5) and (6) and with the results of various measurements to yield values of τ_E and τ_B, the emitter and base effective lifetimes. This has been done as part of a study on a set of specially designed diodes [9].

A second use of Eq. (8) is as a defining relation for an effective gap shrinkage ΔE_G in the emitter. The definition follows directly from the meaning of gap shrinkage employed in [2] and discussed in Chapter II:

$$Q_{EO}/Q_{EO}^{o} \triangleq \exp(\Delta E_G/kT) \tag{9}$$

This definition of ΔE_G agrees exactly with the meaning of $\Delta E_G(x)$ discussed in [2] for the case that the net doping concentration in the quasi-neutral emitter is flat and the emitter minority-carrier lifetime is independent of $\Delta E_G(x)$. For other cases it gives a weighted average of the energy-gap shrinkage over the thickness of the emitter.

III. MEASUREMENTS AND INTERPRETATION

This section treats various measurements that lead to values for τ_B, Q_{BO}, I_{QNO}, and τ_{QN}, which are parameters appearing in Eqs. (5) and (6) of the model described in Section II. That model assumes the dominance of processes occurring in the quasi-neutral emitter and base regions over those located in the junction space-charge region or at the surface. Hence the discussion here will deal with assuring this dominance or, alternatively, with removing from the experimental data that part which belongs to processes in the junction space-charge region and at the surface. A key to appropriate design of experiments and proper treatment of data is the careful linking of that data to the physics governing the observed behavior.

3.1 Device Structures

The discussion of this paper will limit consideration to high-efficiency junction solar cells for which processes occurring in the quasi-neutral emitter contribute significantly to the cell performance. Hence the device structures of interest are made of single-crystal semiconductors, such as silicon. For certain of the measurements - for example, open-circuit voltage and short-circuit current - an entire solar cell may be used. For transient or small-signal measurements, a smaller area is desirable, and the structure used may be part of an entire solar cell or it may be a junction diode specially designed for the purpose. In the measurement of the properties of a dark cell, a diode whose metallization geometry contains an MOS guard ring offers advantages, particularly for n^+-p diodes. A voltage applied to the guard-ring can effectively eliminate the component of current arising from recombination at the surface.

3.2 Base τ_B and Q_{BO}

In the special case of spatially-independent τ_B and N_{AA}, Eq. (7) links τ_B and Q_{BO} together with the diffusion length $L_n = \sqrt{D_n \tau_n}$ of the minority electrons. Both N_{AA} and τ_n may be explored by various measurements of the reverse-biased capacitance C. For example, measuring $1/C^2$ versus V, the reverse bias, determines the value of N_{AA} if it is independent of position. By plotting the same data as $1/C^3$ versus V for small V, one can infer the impurity grade constant a of the junction, which enters in the determination of $N(W_E)$ appearing in Eq. (8).

By various transient-capacitance methods [10] the value of τ_n and its spatial dependence can be found. These methods include:

(a) Thermally-Stimulated Capacitance (TSCAP), which involves measuring high-frequency capacitance versus temperature;

(b) Voltage-Stimulated Capacitance (VSCAP), which involves measuring high-frequency capacitance versus time after a bias voltage change; and

(c) Light-Stimulated Capacitance (LSCAP), which involves measuring high-frequency capacitance versus time after a change in the illumination.

In many junction solar cells τ_n and N_{AA} will be independent of x, validating Eq. (7). For such cells, the diffusion length L_n, and hence the lifetime τ_n, can be independently determined by a technique involving the use of X-rays. In this technique [11] the short-circuit current generated by a uniformly-absorbed beam of 250 KeV X-rays is collected by the junction. This current is nearly proportional to L_n, and a calibrated relation exists [11] for determining L_n.

3.3 Saturation Current I_{QNO}

The parameter I_{QNO} can be inferred either from the static I-V characteristic of a dark diode or from the static I_{SC}-V_{OC} (photo-current versus photo-voltage) response of the diode to various levels of illumination. The key to inferring I_{QNO} from the data lies in the proper linking of that data with the basic mechanisms producing it.

3.3(A) Dark current measurement: The data are taken and plotted as ℓn I versus V. The underlying physics requires that the data follow the relation,

$$I = I_{QNO}[\exp(qV/kT)-1] + I_{XO}[\exp(qV/m_x kT)-1] \quad , \qquad (10)$$

in which the first term describes the component of the current that comes from the quasi-neutral regions and the second term describes the component coming from the bulk [12] and surface space-charge regions [5].

As a first step toward determining I_{QNO}, the observed dependence of ℓn I versus qV/kT is resolved into the two components of Eq. (10). This can be done graphically by subtracting the component involving reciprocal slope m_x, which dominates at low current, from the observed dependence to reveal the component with unity reciprocal slope. This component intersects the ℓn I axis at ℓn I_{QNO}, according to Eq. (10), and the saturation current is thus determined.

The physics underlying Eq. (10) does not include the effects of series resistance or high injection, both of which can bend the curve of ℓn I versus V at high currents, increasing the reciprocal slope. For many highly-doped cells this effect does not obscure the two components of Eq. (10) because the bending occurs at currents several decades higher than the low-current range for which Eq. (10) applies. If a clear separation

does not exist, Eq. (10) must be modified to include the relevant physics [13].

3.3(B) Photo-current measurement: The short-circuit current I_{SC} and the open-circuit voltage V_{OC} are measured at various levels of illumination, and the curve of $\ell n\ I_{SC}$ versus qV_{OC}/kT is plotted. This curve follows the relation,

$$I_{SC} = I_{QNO}[\exp(qV_{OC}/kT) - \exp(qI_{SC}R_S/kT)] + I_{XO}[\exp(qV_{OC}/m_x kT) - \exp(qI_{SC}R_S/m_x kT)] \quad (11)$$

which is consistent with the underlying physics. For completeness, the effect of a series resistance R_S is included, but Eq. (11) must be modified further if the effects of high injection should prove to be significant in a particular cell. As in the treatment of the dark-current data, the measured dependence is resolved into the two components given in Eq. (11). Then I_{QNO} is the intercept on the $\ell n\ I_{SC}$ axis made by the component with unity reciprocal slope.

3.3(C) Temperature Dependence: As an alternate method for determining I_{QNO} and as a check against the results of the methods just described, the current-voltage dependence can be measured at temperatures higher than 300°K. The component of current coming from the quasi-neutral regions is approximately proportional to n_i^2, which in turn is proportional to $\exp(-E_G/kT)$, where E_G is the band gap. In contrast, the components arising from processes other than those located in the quasi-neutral regions are approximately proportional to n_i rather than n_i^2 and thus to $\exp(-E_G/2kT)$ rather than $\exp(-E_G/kT)$. Accordingly, as temperature rises the component of current from the quasi-neutral regions will tend to become more dominant and the measured dependence will tend more toward unity

slope. At a high enough tmeperature, the measured dependence will show practically unity slope, and I_{QNO} can be found without the need to separate the current-voltage characteristic into the quasi-neutral and space-charge components.

3.4 Relaxation time τ_{QN}

The response to any time-varying excitation will contain information about the relaxation time τ_{QN}. Three methods of excitation that have received some attention in the past will be discussed here as means for determining τ_{QN}. The three methods are:

(a) Junction current recovery [14], or JCR, in which the dark diode is first forward biased to set the initial charges residing within the device, and then a reverse current is applied to speed the decay of these charges.

(b) Open-circuit voltage decay [15], or OCVD, in which the initial charges are set as in JCR but then are allowed to relax in the open-circuited condition with no reverse current applied.

(c) Admittance vs. frequency [16], in which a small sinusoidal excitation imposed on the bias condition is applied and the real and imaginary parts of the complex admittance are measured as functions of frequency and bias.

The relaxation time τ_{QN} governs the force-free response of the model of Section II, in which the charge of the mobile carriers within the quasi-neutral regions is assumed dominant over that within the bulk and surface space-charge regions. Therefore, if the quasi-neutral regions

dominate, the OCVD response directly gives τ_{QN}. The OCVD method has an advantage over the JCR method because JCR necessarily involves an excursion over the entire range of forward voltages including that range in silicon diodes for which the space-charge region will dominate in producing the response. Hence the relaxation time inferred from JCR data will differ from τ_{QN}. In contrast, the initial linear portion of the OCVD response, from which the relaxation time is deduced, can derive from processes located in the quasi-neutral regions, and thus can determine τ_{QN}.

Whether the processes in the quasi-neutral regions dominate in producing the dynamic response is disclosed by the dependence on bias voltage seen in the real and the imaginary parts of the measured admittance [17]. Increasing the temperature will increase the dominance of the quasi-neutral regions, for much the same reasons as in Section 3.3(c).

3.5 Other Measurements

The measurements discussed above are electrical. Other measurements, electrical and non-electrical, could be taken with possible advantages. The of measurements given here is meant to be suggestive, not exhaustive.

3.6 Internal Consistency and Measurement Sensitivity

The experimental results yielded by these various measurements overlap. Because they are not mutually exclusive, some checks can be made for internal consistency. For example, from Eqs. (5) and (6) alone it follows that:

$$\Delta \triangleq Q_{EO}/Q_{BO} = \frac{\tau_{QN} I_{QNO}}{Q_{BO}} - 1 \ , \tag{12}$$

$$\tau_B/\tau_E = (1/\Delta)\left[(\tau_B/\tau_{QN})(\Delta+1) - 1\right] \tag{13}$$

where $\Delta = Q_{EO}/Q_{BO} = [\exp(\Delta E_G/kT)]Q^{o}_{EO}/Q_{BO}$ is a measure of the gap shrinkage.

Alternatively, expressions for Δ and τ_B/τ_E can be developed that relate to V_{OC} and I_{SC}, the measured open-circuit voltage and short-circuit current of the illuminated cell. To develop these, we use [18]

$$\exp[-qV_{OCqn}/kT] \simeq I_{QNO}/I_{SC} \ . \tag{14}$$

Here V_{OCqn} is the open-circuit voltage that would occur in a solar cell if the dark current resulted from recombination only in the quasi-neutral regions. In other words, V_{OCqn} is the open-circuit voltage of an idealized solar cell for which the second term in Eq. (10), representing space-charge-layer recombination, is negligible when $I = I_{SC}$. To correct for the presence of recombination in the bulk and surface space-charge layers, the expression

$$qV_{OCqn}/kT = qV_{OC}/kT + \ell n\left[\frac{I_{SC}}{I_{QNO}\exp(qV_{OC}/kT)}\right] \tag{15}$$

relates the measured voltage V_{OC} to the idealized voltage V_{OCqn}. This expression follows directly from inspection of the graph of the two components of I in Eq. (10). The two components are determined from the measured current-voltage dependence as explained in Section 3.3(A).

The voltage V_{OCqn} accounts for recombination in both the quasi-neutral base and emitter regions. We identify

$$V^{B}_{OCqn} = \frac{kT}{q}\,\ell n\left[\frac{I_{SC}}{Q_{BO}/\tau_B}\right] \tag{16}$$

as the open-circuit voltage if recombination in the base alone were important, and

$$\delta V_{OC} = V^{B}_{OCqn} - V_{OCqn} \qquad (17)$$

as the shift in open-circuit voltage resulting from significant recombination in the emitter. Note that δV_{OC} is positive. Combining Eqs. (5) and (6) with (14) through (17) yields

$$\Delta = \frac{\exp(q\delta V_{OC}/kT)}{\tau_B/\tau_{QN}} - 1, \qquad (18)$$

$$\tau_B/\tau_E = (1/\Delta)[\exp(q\delta V_{OC}/kT) - 1] , \qquad (19)$$

which are the desired expressions.

Eqs. (12) and (18) provide two alternative calculations of Δ, and hence of the gap shrinkage. Eqs. (13) and (19) provide two alternative means for calculating the emitter lifetime. None of these four relations depends strongly on the intrinsic concentration, n_i. This is desirable because n_i and its temperature dependence is not accurately known at present. In contrast to Eqs. (18) and (19), note that the use of Eqs. (12) and (13) does not necessarily require measurements under illumination. This indicates that the two methods of calculation are, to some degree, independent. As part of the methodology we require for any device under study that the calculations of Δ by Eqs. (12) and (18) agree satisfactorily, and that the calculations of τ_E by Eqs. (13) and (19) likewise agree. Expressed in general terms, internal consistency is required.

Eqs. (12) and (18) in effect express the charge Q_{EO} as the difference between the charge Q_{BO} and the total (excess minority-carrier) charge, $Q_{EO} + Q_{BO}$ For some devices--for example, those in which gap shrinkage is small--these two equations call for the determination of Q_{EO} by subtracting two numbers that nearly are equal. Because some uncertainty will always exist about the measured values used in these calculations, the method will give no accuracy in the calculation of Q_{EO} (or Δ) for these cases.

The measurement sensitivity of the effective gap shrinkage and lifetime of the emitter thus depends on the accuracy with which each of the measured quantities---I_{QNO}, τ_{QN}, Q_{BO}, τ_B, V_{OC}, and I_{SC}-- are determined. Let Δ_{min} be the minimum value of Δ that can be determined for a certain precision of the measurements. (For example, if $\Delta_{min} = 1$, it is assumed that Q_{EO} can be determined from Eqs. (12) or (18) only if $Q_{EO} \geq Q_{BO}$.) Then, from Eq. (8) and the definition of Δ, the minimum determinable value of the gap shrinkage $\Delta E_{G_{min}}$ is

$$\Delta E_{G_{min}} = kT\ell n[\Delta_{min} Q_{BO}/Q_{EO}^{o}] \tag{20}$$

$$= kT\ell n\{(\Delta_{min} L_N/W_E\ \ell n[N_{MAX}/N(W_E)]$$

This is defined as the measurement sensitivity for the gap shrinkage of a given device. Similarly, combining Eq. (20) with Eqs. (13) or (19), we can define the corresponding measurement sensitivity for the emitter lifetime.

3.7 Path Toward Greater Measurement Sensitivity

From Eq. (20) we note that increasing $\Delta_{min} L_n/W_E$ will give the greatest increase in measurement sensitivity. Eqs. (12) and (18) imply that the quanti Δ_{min} is set by the precision with which τ_{QN}, I_{QNO}, L_n, N_{AA}, V_{OC}, and I_{SC} are measured. The emitter thickness W_E can be purposefully increased in cells especially designed to explore the gap shrinkage experimentally. Some evidence exists that the diffusion length L_n decreases rapidly with increasing doping concentrations N_{AA} in the base for $N_{AA} > 10^{18} cm^{-3}$. Hence, increasing the conductivity of the base region could much improve the sensitivity. Alternatively, the diffusion length can in effect be shorter by structural and electrical means through adding a collector region, making a transistor-like structure. The third terminal that can be contacted to such structures also provides for a direct and accurate measurement of τ_E, from which Q_{EO} and the gap shrinkage can be deduced [19].

IV. ILLUSTRATIVE EXAMPLE

4.1 Device Fabrication

Six n^+-p silicon solar cells shown in Fig. 2 were constructed at NASA Lewis Research Center using a standard processing technique. The 1 x 2 cm, vacuum-float-zone, <111> orientation, 0.1 ohm-cm (approximately), p-type silicon wafers were first chemically polished in an HF-HNO_3 - glacial acetic acid solution. The wafers were then phosphorus diffused in a $POCl_3$ atmosphere for 45 minutes at a temperature of 880°C to form the n^+-p junction. The junction depth is about 0.25μm and the surface concentration is about $2x10^{20} cm^{-3}$. After removal of the phosphorus oxide glass with HF, silver-aluminum contacts were thermally evaporated to form the large area contact to the p-type silicon substrate and the gridded contact to the thin diffused layer. Contact adherence was insured by sintering the cells in argon at 550°C for several minutes.

For the measurements involving illumination, the entire solar-cell structure was used. Mesa structures of small area ($3.5x10^{-4}$ cm^2) were etched for use in the dark-current and the OCVD measurements.

4.2 Measurements and Calculations

To illustrate the methodology, we describe here the measurements and cal tions made for a typical sample. The data were taken at temperature T = 295.

First the material parameters for the base are found. From the X-ray method L_n = 82 microns, and from measuring the reverse-biased capacitance the doping concentration is deduced to be $N_{AA} = 2x10^{17} cm^{-3}$. From standard references [20], this implies a diffusivity, D_n = 10 cm^2/sec, and hence a lifetime, τ_B = 6.7 microseconds. From Eq. (7), $Q_{BO} = 5.4x10^{-19}$ C/ At this point we also calculate $Q^o_{EO} = 2.4x10^{-22}$ C/cm^2, from Eq. (8).

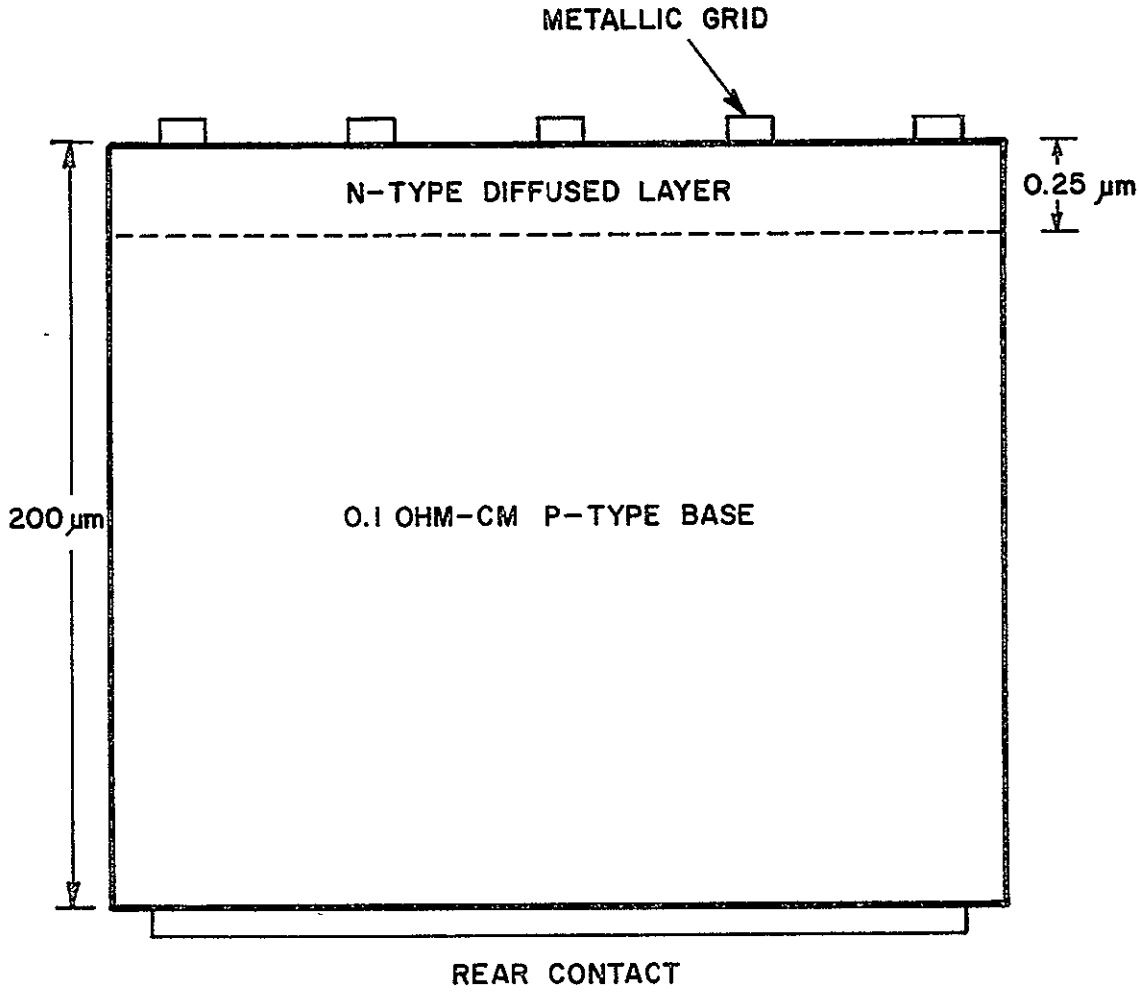

Fig. 2 Cross section of silicon solar cell used in this study.

The remaining parameters are measured as described in Section III. By the OCVD method, τ_{QN} = 0.67 μsec. The current-voltage measurements made on a dark diode give $I_{QNO} = 1.1 \times 10^{-12} A/cm^2$. This value agrees well with that determined from illuminated current-voltage characteristics measured using a calculator-controlled-data-acquisition system. A xenon-light solar simulator used for the AMO (outer-space condition) measurements yields V_{OC} = 0.600 volts and I_{SC} = 23 mA/cm^2. The data also give δV_{OC} = 67mV as the voltage shift defined in Eq. (17).

From these data, the calculations of the gap shrinkage and the emitter lifetime can be made. First, using data secured only from the response of the dark device, we find from Eq. (12) that $\Delta = 0.38$ (implying $Q_{EO} = 2 \times 10^{-19} C/cm^2$ and ΔE_G = 170meV) and from Eq. (13) that $\tau_B/\tau_E = 34$ (implying τ_E = 195nsec). Second, using data secured by measurements using illumination, we find from Eqs. (18) and (19) nearly the same values for Δ, ΔE_G, and τ_E.

4.3 Interpretation of Results

The results of Eqs. (12) and (18) for the effective gap shrinkage agree well, so do the results of Eqs. (13) and (19) for the effective emitter lifetime. Moreover, alternate methods used for determining I_{QNO} and τ_{QN} show good agreement. Hence, as discussed in Section 3.6, the requirement of internal consistency among the measurements is met.

Consider now the measurement sensitivity, treated in Section 3.6. If 5% accuracy is assumed in the measurement of each parameter (I_{QNO}, τ_{QN}, and Q_{BO}) in Eq. (12), then the minimum detectable value of Δ is $\Delta_{min} \simeq 0.15$. From Eq. (20), this corresponds to $\Delta E_{G_{min}} \simeq$ 147meV the minumum detectable value of the gap shrinkage for the particular solar-cell structures treated. The results obtained here are $\Delta = 0.38$ and ΔE_G = 170meV which lie within this assumed measurement sensitivity.

Greater measurement sensitivity is desirable, however, and to increase the sensitivity we have undertaken all of the three approaches indicated in Section 3.7. The results of these studies and a detailed consideration of the measurement accuracy and sensitivity will be reported elsewhere.

We emphasize that the methodology described here determines τ_E and Q_{EO}, the effective lifetime and the minority-carrier charge stored in the emit These two variables are fundamental in the sense that the values determined for them are independent of the specific physical mechanisms assumed in the physical model describing the degenerately doped emitter. If one uses a physical model for the emitter that <u>assumes</u> the presence of energy gap shrinkage, then a simple measure of the effective gas shrinkage can be calculated from Eq. (9). But the fact that the experimentally determined value of Q_{EO} much exceeds the value Q_{EO}^{o} calculated assuming the absence of gap shrinkage, as is true for the cell studied here, does not itself <u>prove</u> the existence of sizable energy-gap shrinkage. Rather it can only show <u>consistency</u> with a physical model containing energy-gap shrinkage.

A less fundamental problem in interpretation also deserves mention. If Eq. (9) is used to relate Q_{EO} to ΔE_G, then Q_{EO}^{o} must be calculated. That requires knowledge of the doping concentration profile $N_{DD}(x)$ in the quasi-neutral emitter and, for a shallow-junction cell, it may require knowledge al of the effective surface recombination velocity at the front surface. If $N_{DD}(x)$ has a large enough gradient over a considerable part of the quasi-neutral emitter, the resulting built-in electric field causes Q_{EO}^{o} to be practically independent of the lifetime $\tau_p(x)$ and of the surface recombination velocity s. Then Q_{EO}^{o} is given by Eq. (8) and the value for ΔE_G stated above (170 meV) holds. But if $N_{DD}(x)$ were nearly flat over practically the entire quasi-neutral emitter, then the calculation of Q_{EO}^{o} would require $\tau_p(x)$ and s. For this case, if the emitter were transit-time limited

rather than lifetime limited, Q_{EO}^{o} could be considerably larger than the value calculated above and ΔE_G could be considerably smaller.

REFERENCES FOR CHAPTER IV

1. W. Shockley, "The theory of p-n junctions in semiconductors and p-n junction transistors," Bell Sys. Tech. J., vol. 28, pp. 435-489, July 1949.

2. F.A. Lindholm and C.T. Sah, "Fundamental electronic mechanisms limiting the performance of solar cells," IEEE Trans. Electron Devices, this issue.

3. H.W. Brandhorst, Jr., "Current status of silicon solar cell technology," Technical Digest, 1975 Int. Electron Devices Meeting (75CH1023-1 ED), pp. 331-338, Dec. 1975.

4. F.A. Lindholm and C.T. Sah, "Normal modes of semiconductor pn junction devices for material-parameter determination," J. Appl. Phys., vol. 47, pp. 4203-4205, Sept. 1976.

5. C.T. Sah, "Effect of surface recombination and channel on p-n junction and transistor characteristics," IRE Trans. on Electron Devices, vol. ED-9, pp. 94-108, Jan. 1962.

6. E.O. Johnson and A. Rose, "Simple general analysis of amplifier devices with emitter, control, and collector functions," Proc. IRE, vol. 47, pp. 407-418, March 1959.

   R.D. Middlebrook, "A modern approach to semiconductor and vacuum device theory," IEEE Proc., vol. 106B, suppl. 17, pp. 887-902, March 1960.

   P.E. Gray, D. DeWitt, A.R. Boothroyd, and J.F. Gibbons, Physical Electronic and Circuit Models of Transistors, Wiley, New York, 1964.

7. F.A. Lindholm, "Simple expressions for the minority-carrier charge in the emitter of p-n-junction devices," to be published.

8. F.A. Lindholm, S.S. Li, and C.T. Sah, "Fundamental limitations imposed by high doping on the performance of pn junction silicon solar cells," Record 11th Photovoltaic Specialists Conf., (75CH0948-0ED), pp. 3-12, 1975.

9. A. Neugroschel, F.A. Lindholm, and C.T. Sah, "A method for determining the emitter and base lifetimes in p-n-junction diodes," IEEE Trans. Electron Devices, submitted for publication.

10. C.T. Sah, L. Forbes, L.L. Rosier, and A.F. Tasch, Jr., Solid-State Electronics, vol. 13, pp. 759-788, June 1970. See also reviews treating these and more recent methods in C.T. Sah, "Bulk and interface imperfections in semiconductors," Solid-State Electronics, in press, and C.T. Sah, "Detection of recombination centers in solar cells from junction capacitance transients, IEEE Trans. Electron Devices, this issue.

11. J.H. Lamneck, Jr., "Diffusion lengths in silicon obtained by an X-ray method," NASA TM X-1894, Oct. 1969.

12. C.T. Sah, R.N. Noyce, and W. Shockley, "Carrier generation and recombination in p-n junctions and p-n junction characteristics," Proc. IRE, vol. 45, pp. 1228-1243, Sept. 1957.

13. M. Wolf and H. Rauschenbach, "Series resistance effects on solar cell measurements," Advanced Energy Conversion, vol. 3, pp. 455-479, Apr.-June 1963.

14. R.H. Kingston, "Switching time in junction diodes and junction transistors," Proc. IRE, vol. 42, pp. 829-834, May 1954.

H.J. Kuno, "Analysis and characterization of p-n junction diode switching," IEEE Trans. on Electron Devices, vol. ED-11, pp. 8-14, Jan. 1964.

15. S.R. Lederhandler and L.J. Giacoletto, "Measurement of minority carrier lifetime and surface effects in junction devices," Proc. IRE, vol. 43, pp. 477-483, April 1955.

16. W. Shockley, Electrons and Holes in Semiconductors, pp. 313-318, Van Nostrand, Co., New York, 1950.

H. Maes and C.T. Sah, "Application of the equivalent circuit model for semiconductors to the study of Au-doped p-n junctions under forward bias," IEEE Trans. Electron Devices, Vol. ED-23, pp. 1131-1143, Oct. 1976.

17. F.A. Lindholm and M.B. Callaway, to be published; also C.T. Sah, "Effects of Electrons and Holes on the Transition Layer Characteristics of Linearly-Graded p-n Junctions," Proc. IRE, vol. 49, pp. 603-618, March 1961.

18. M.B. Prince, "Silicon Solar energy converters," J. Appl. Phys., vol. 26, pp. 534-540, May 1955.

19. A. Neugroschel, F.A. Lindholm, and C.T. Sah, "Experimental determination of emitter lifetime and band-edge distortion in transistors," Electronic Letters, to be published.

20. M.B. Prince, "Drift mobilities in semiconductors. II. Silicon," Phys. Rev., vol. 93, pp. 1204-1206, March 1954.

S.M. Sze and J.C. Irvin, "Resistivity, mobility, and impurity levels in GaAs, Ge, and Si at 300°K," Solid-State Electron., vol. 11, pp. 599-609, 1968.

CHAPTER V. DISCUSSION

This research program concentrates on the open-circuit voltage in (n-on-p) single-crystal silicon p-n junction solar cells of 0.1 ohm-cm substrate resistivity. The purpose is to explain, in fundamental terms, the reasons for the discrepancy that exists between observed values of the open-circuit voltage and those predicted by traditional theory--a discrepancy of about 100 mV.

In Chapter I, we identified anomalous values of the stored minority-carrier charge Q_{EO} and of the phenomenological lifetime τ_E in the emitter of the solar cell as the probable origins of this discrepancy. In Chapter II, proceeding from a theoretical standpoint, we identified high recombination rates and effective gap shrinkage in the quasi-neutral emitter region as the two main fundamental electronic mechanisms responsible for the discrepancy in a one-dimensional model of the solar cell, and noted the possible role of areal inhomogeneity in contributing to the discrepancy. We examined the many mechanisms that can give rise to high recombination rates (low lifetime) and to gap shrinkage (large minority-carrier storage). The lack of relevant experimental data and the inadequacies of the existing theoretical models prevented our reaching firm conclusions about the role of low lifetimes compared with that of gap shrinkage in producing the V_{oc} discrepancy. Thus, we turned to the problem of experimentally determining the effective lifetime and effective gap shrinkage in the emitter. Our findings are described in Chapters III and IV.

Although our objective in the research program focusses on n-on-p solar cells, the technical findings reported in Chapter III come from

measurements made on p^+-n diodes. We chose a p^+-n structure for our initial experiments for three reasons:

(1) The charge in the oxide covering the semiconductor surface invariably is positive. Hence surface channels and consequent recombination that obscure the bulk recombination being studied tend to occur more in n^+-p devices than in p^+-n devices. This surface channeling can be pinched-off by application of guard-ring voltages, but the study of p^+-n devices remains easier than that of n^+-p devices.

(2) Schottky-barrier metal-semiconductor junctions must be made to find the density of imperfection centers in the substrate prior to junction fabrication. These enable study of the imperfections caused by the processing used in junction fabrication. Schottky barriers can be easily made on n material, using aluminum as the metal. For p material, the choice of metal becomes a problem of finding one that will yield a sizeable barrier height yet remain stable. Although not insurmountable, this problem makes the study of p^+-n cells easier.

(3) Transient-capacitance and related measurements applied to a p^+-n cell readily and simply yield information about the imperfection centers that lie in the upper half of the band gap. These centers control the minority carrier lifetime in the substrate of an n^+-p cell, and thus study of p^+-n structures yields information of direct relevance to the characterization of n-on-p solar cells.

Of these reasons, the third was the most important in our choice to study n^+-p devices first. The motivation was to get relevant information as quickly and easily as possible while developing understanding and experimental procedures that could be later applied (Chapter IV) to n^+-p structures.

Additionally, to get concrete results fast, and being aware of the potential problems in sensitivity of measurements done directly on material of 0.1 ohm-cm resistivity made at low diffusion temperatures, we fabricated structures of different doping densities in the base (10^{14} to 10^{17} cm^{-3}) using different diffusant temperatures (900° to 1200°C). Although temperatures above 900°C are rarely used in solar-cell fabrication, the high-temperature treatment tends to create many imperfections that can be easily measured even on a highly-doped substrate.

In Chapter III, a method was described that provides an experimental means for the first time to separate and determine the emitter and base lifetimes in a p-n junction diode after the junction has been fabricated. In the method, several static and transient measurements were analyzed using physical models of the diode characteristics. To illustrate the method, diffused silicon diodes were fabricated having substrate (base) impurity concentrations ranging from 10^{14} to nearly 10^{17} phosphorous atoms per cubic centimeter. The results show an emitter lifetime that is much smaller than the base lifetime in the diode having the highest base doping concentration. In this diode, the recombination current from the emitter is 65% of the recombination current from the base, demonstrating the significance of the emitter in governing the static current-voltage dependence. The importance of emitter recombina-

tion to the transient characteristics was also demonstrated. Chapter III emphasized the techniques by which the base and emitter lifetimes are distinguished. It also demonstrated the need for carefully basing the quantitative analysis of the measurements on the underlying diode physics.

The work of Chapter IV builds on the understanding and the procedures developed in Chapter III. The methodology described in Chapter IV provides the first means available for the experimentally-based determination of the minority-carrier charge Q_{EO} (effective gap shrinkage) and the effective lifetime in the emitter of p-n-junction solar cells. It also makes available for the first time a means for determining these material parameters in the emitter of any p-n-junction device. Its use was illustrated in the chapter by applying it to an n^+-p solar cell of 0.1 ohm-cm substrate resistivity.

The methodology contrasts with the recent experimental study of bandgap shrinkage due to Slotboom and De Graaf [1]. That study restricted attention to gap shrinkage in the highly-doped base region of bipolar transistors. As a consequence the doping concentrations studied did not exceed 2×10^{19} cn^{-3}; and p-type dopants only were considered in the particular study reported. In contrast the methodology described in Chapter IV determines the gap shrinkage in the emitter itself. It thus emphasizes the effects of the mechanical strain and of the very degenerate doping concentrations ($N_{DD} >> 10^{19}$ cm^{-3}) occurring near the diffused emitter surface. These effects could be significant, particularly in shallow-junction emitters. In addition to the gap shrinkage, the methodology determines the effective carrier lifetimes in the base and the emitter. As is discussed in Chapter II, the emitter lifetime is

also likely to be sensitive to the effects of mechanical strain and degenerate doping concentrations occurring near the surface.

Because of these differences, the methods of Slotboom and De-Graaff and those presented here will likely give different results, and a comparison is in order. In their Eq. (18), Slotboom and De Graaf give an empirical fit for gap shrinkage versus doping concentration. This fit holds for regions far from the surface, for p-type dopants, and for doping concentrations less than 2×10^{19} cm^{-3}. But if the fit is nevertheless applied to the solar cell studied in Section IV, it yields the following values for the gap shrinkage in the shallow n-type emitter:

$$\Delta E_G = 125 \text{ meV for } N_{DD} = 10^{20} cm^{-3} \text{ and } \Delta E_G = 135 \text{ meV for } N_{DD} = 2\times10^{20} cm^{-3}$$

These values are smaller than the gap shrinkage of 170 meV found from the methodology of Chapter IV. The approach of Slotboom and DeGraaff does not concern itself with lifetimes, which the methodology gives as $\tau_B = 6.7\mu sec$ and $\tau_E = 195$ nsec for the particular cell studied.

The methodology consists of a strategy for designing experiments and interpreting data consistently with the physical mechanisms governing device behavior. It is based on a model that has the following properties:

(a) it describes both the static and the dynamic response;

(b) it describes the device both in the dark and under illumination;

(c) it characterizes the part of the device behavior coming from the surface and the bulk space-charge regions;

(d) it accounts for contributions to the device behavior coming from the quasi-neutral emitter as well as from the quasi-neutral base.

As this model recognizes, many aspects of device behavior can come from processes not occurring within a single region of the device. But, for high-quality silicon solar cells, the short-circuit current flowing in response to X-rays originates mainly in the quasi-neutral base region. Combining this response with the several other measurements indicated in Section 3.2 of Chapter IV fixes the value of the base lifetime τ_B and the related charge Q_{BO}. The determination of these parameters of the base helps toward the determination of lifetime and gap shrinkage in the quasi-neutral emitter. But the contribution to device behavior coming from the space-charge regions must be removed because it obscures that coming from the emitter. Several procedures are described for removing this contribution. They involve structural and electrical means, such as the use of an MOS guard ring, or heating the device, or resolving the data into components. The results of these procedures are then substituted into Eqs. (12) or (18) for the gap shrinkage in the emitter, and into Eqs. (13) or (19) for the emitter lifetime.

For the n^+-p cell structure studied in Chapter IV, the emitter plays a decisive role in determining solar-cell performance. The importance of the emitter has been suggested in earlier papers, but the experimental results given in Chapter IV provide direct evidence of this importance. For example, note that $\tau_B/\tau_{QN} \simeq 10$. Thus the relaxation time τ_{QN} measured by any of the methods discussed in Section 3.4 differs greatly from the effective base lifetime τ_B. As was indicated in Chapter III, only for diodes with low base doping concentrations will $\tau_B \simeq \tau_{QN}$.

The treatment in Chapter IV has ignored the effects of areal inhomogeneity, which were described in Chapter II. These effects can be studied by applying the methods of this chapter to many small-area

device structures scribed from a large-area wafer subjected to solar-cell processing.

The methodology of Chapter IV bears on the engineering design of solar cells. It constitutes part of an effort to discover and describe the fundamental electronic mechanisms (Chapter II) influencing solar-cell efficiency, and to provide mathematical models that incorporate these mechanisms into solar-cell design. The methodology yields the excess minority-carrier charge stored in the emitter and the lifetimes in the emitter and the base. If the values of these parameters thus determined are correct, then any physical model that truly describes the cell must predict behavior consistent with these values. Because computer solution of the relevant differential equations is possible, physical models of any degree of complexity can be studied--models containing various combinations of the fundamental electronic mechanisms (Chapter II) that could influence device behavior. Comparison between the experimentally-based results of the methodology and the results predicted by computer simulation can then disclose which of the fundamental mechanisms dominate in determining the cell efficiency. We have begun work aiming toward such a comparison.

The work of Chapter IV relates mainly to the mechanisms of band-edge distortion and high recombination rates present in the diffused emitter. By providing methods for quantitatively determining these mechanisms, that work enables study of their relations to the processing used in solar-cell fabrication. It thus leads toward a systematic improvement of open-circuit voltage and cell efficiency. A systematic study of the relations between processing and the electronic mechanisms

controlling efficiency is under way, and we plan to report the results of this study elsewhere.

REFERENCES FOR CHAPTER V

J. M. Slotboom and H. C. De Graaff, "Measurements of bandgap narrowing in Si bipolar transistors," Solid-State Electron., vol. 19, pp. 857-862, Oct. 1976.

List of Symbols

D_n, D_p	Electron and hole diffusivities
$\Delta N, \Delta P$	Excess electron and hole densities
E	Electric field
ε	Dielectric permittivity
G_N^O, G_P^O	Optical generation rates of electrons and holes
J, I	Solar cell current density, current
J_D, I_D	Dark diode current density, current(subscript 0 denotes saturati curre
J_N, J_P	Electron and hole current densities
J_{SC}, I_{SC}	Short-circuit current density, current
J_{UPC}	Uncompensated photocurrent density
k	Boltzmann's constant
μ_n, μ_p	Electron and hole mobilities ($b = \mu_n/\mu_p$)
N, P	Electron and hole densities
N_{AA}, N_{DD}	Ionized acceptor and donor impurity concentrations
n_i	Intrinsic carrier density
N_T	Negatively-charged trap density
q	Electron charge
R_N, R_P	Electron and hole steady-state recombination rates for thermal processes
R_S	Series resistance
ρ	Space charge density
T	Absolute temperature
V	Solar-cell terminal forward voltage
V_B	Quasi-neutral base region voltage
V_I	Intrinsic Fermi potential (or electrostatic potential)
V_J	Junction space-charge region voltage
V_N, V_P	Electron and hole quasi-Fermi potentials

I. INTRODUCTION

Conventionally, the current in an illuminated solar cell is described by the dark current-voltage characteristic $I_D(V)$ shifted by the measured short-circuit current I_{SC}:

$$I(V) = -I_D(V) + I_{SC} \tag{1}$$

This description has served as a basis for many past theoretical estimates of various measures of solar cell performance. As is explained in Chapter I, the separation of I(V) into the components of (1) is useful because it essentially reduces the problem of explaining the V_{OC} discrepancy to the problem of understanding $I_D(V)$, the *dark* current-voltage characteristics.

As we show in this Appendix, however, the fundamental reasons justifying (1) hold only under restricted conditions. The use of (1) beyond its range of validity can lead to sizable errors in predicting the electrical characteristics of solar cells and thus to misleading conclusions about design. The shifting approximation holds, however, for the 0.1 ohm-cm silicon cells of interest in this research program.

The appendix has several purposes:

(a) To define the range of validity of (1) from fundamental consideration of the relevant boundary-value problems;

(b) To note instances of practical importance for which the use of (1) will yield erroneous conclusions concerning cell performance;

(c) To demonstrate, by laboratory experimentation and by exact computer solution of the pertinent boundary-value problems, the errors that can result from the use of (1); and

(d) To develop approximate analytic expressions for cell performance, based on the device physics, that hold when (1) fails to apply.

Despite the widespread use of (1), it has apparently, until now, been justified only from an intuitive standpoint; no rigorous derivation of it has yet been done. In this Appendix, we provide such a derivation. The derivation is based on the *principle of superposition*, which applies if and only if the relevant boundary-value problems are linear.

Following this derivation, we consider several examples of cell operation for which superposition and (1) do not apply. In these examples, we treat the effects of: (a) optical generation and net thermal recombination in the junction space-charge region; (b) high-injection concentrations of holes and electrons; and (c) series resistance. The treatment of high injection involves consideration of cells in concentrated sunlight. Exact computer solutions of the boundary-value problems underlying cell operation together with laboratory experimentation are used to support the theoretical developments.

II. APPLICABILITY OF THE SUPERPOSITION PRINCIPLE TO SOLAR CELLS

If a system is linear, its response to several excitations is the sum of the responses to each excitation applied alone. This is the principle of superposition, which is a basic theorem of linear differential equations [1] and which is widely used in such fields as electrical circuit theory [2] and control systems [3].

We now apply the principle of superposition to a p-n-junction solar cell. As chapter II discusses, the fundamental equations describing this system in the dc steady state are [4,5]:

$$\vec{J}_N = +qD_n \nabla N + q\mu_n N\vec{E} \tag{2}$$

$$= -q\mu_n N \nabla V_N \tag{2a}$$

$$\vec{J}_P = -qD_P \nabla P + q\mu_P P\vec{E} \tag{3}$$

$$= -q\mu_P P \nabla V_P \tag{3a}$$

$$0 = +\nabla \cdot \vec{J}_N + q(G_N^O - R_N) \tag{4}$$

$$0 = -\nabla \cdot \vec{J}_P + q(G_P^O - R_P) \tag{5}$$

$$\nabla \cdot \vec{E} = -\nabla^2 V_I = (\rho/\varepsilon) = (q/\varepsilon)\ (P - N + N_{DD} - N_{AA} - N_T) \tag{6}$$

$$\vec{J} = \vec{J}_N + \vec{J}_P \ . \tag{7}$$

In general, this set of equations is nonlinear. Thus superposition does not apply unless approximations are made that remove the nonlinearity from the system description.

The first approximation to be made follows the widely-used Shockley method of analysis [4] which divides the cell into three coupled systems: the quasi-neutral emitter (QNE) and quasi-neutral base (QNB) regions, and the junction space-charge region (SCR) that separates them. The total current density J drawn from the cell results from the recombination-generation processes in the three regions. To demonstrate this for the one-dimensional n^+-p solar cell of Fig. 1, we integrate the hole continuity equation, (5), over the entire cell to obtain

$$J_P(W_B) - J_P(-W_E - W_{SCR}) = q\int_{QNE}(G_P^O - R_P)\,dx + q\int_{SCR}(G_P^O - R_P)\,dx + q\int_{QNB}(G_P^O - R_P)\,dx \ . \tag{8}$$

Because of the Ohmic contact present at the back surface ($x = W_B$),

$$J = J_P(W_B) \ . \tag{9}$$

The high recombination rates that occur in many cells near the illuminated surface ($x = -W_E - W_{SCR}$) imply that

$$|J| >> |J_p(-W_E - W_{SCR})| \quad . \tag{10}$$

For the dc steady state, in general,

$$G_P^O - R_P = G_N^O - R_N = G^O - R \quad . \tag{11}$$

Thus, using Eqs. (9), (10) and (11), we write (8) as

$$J = q\int_{QNE}(G^O - R)\,dx + q\int_{SCR}(G^O - R)\,dx + q\int_{QNB}(G^O - R)\,dx$$

$$\triangleq J_{QNE} + J_{SCR} + J_{QNB} \tag{12}$$

Eq. (12) is analogous to Kirchoff's current law of electric circuit theory [2], as is illustrated in the equivalent-circuit representation of Fig. 2. Eq. (12) and Fig. 2 are valid regardless of whether or not superposition can be applied to the system describing the solar cell.

We now examine the applicability of superposition to each of the regions of the cell. Consider first the quasi-neutral emitter and base regions. If low-injection conditions prevail in the quasi-neutral regions and the effects of series resistance are negligible, then the expressions for the minority-carrier current and the net thermal recombination rate R both become linear in the minority-carrier concentration. Thus the continuity equation for minority carriers, (4), is linear, and the principle of superposition applies. The linearity of the system holds in general despite the presence of built-in electric fields arising from impurity concentration gradients and despite heavy-doping effects [5] in the emitter such as energy-band-edge distortion.

To illustrate the use of superposition, consider the p-type base region of the solar cell of Fig. 1. For this system the independent excitations are the optical generation rate $G^O(x)$ and the excess minority-carrier (electron) concentration $\Delta N(0)$. The response is the minority-carrier current J_{QNB} of (12). Combining (11) and (12), we write

$$J_{QNB} = q\int_{QNB} (G_N^O - R_N)\,dx \tag{13}$$

which is linearly related to the minority-carrier concentration and to the optical generation rate. Thus, using superposition, we obtain

$$J_{QNB} = J_{QNB}\Big|_{\substack{G_N^O = 0 \\ \Delta N(0) \neq 0}} + J_{QNB}\Big|_{\substack{G_N^O \neq 0 \\ \Delta N(0) = 0}} \tag{14}$$

The first term of (14) is a dark current $-J_{QNB}^D$. The second term is a photocurrent J_{QNB}^O. Therefore,

$$J_{QNB} = -J_{QNB}^D + J_{QNB}^O, \tag{15}$$

which can be represented by the equivalent circuit of Fig. 3. This decomposition of J_{QNB} focuses attention on the dark current component, which is given by [4]

$$J_{QNB}^D = J_{QNBO}^D\,(e^{qV/kT} - 1) \tag{16}$$

for the assumed conditions of low injection and neglibible series resistance.

Analogous results describe the current J_{QNE} from the quasi-neutral emitter. Thus, if superposition applies, the component of current from the two quasi-neutral regions has the form of (1); it consists of a dark-current characteristic shifted by a photocurrent.

We now consider the applicability of superposition to the junction space-charge region. In this region the electric field E depends on the hole and electron concentrations, N and P. This introduces nonlinearity into the current density expressions, (2) and (3). Furthermore, the net thermal recombination rates, R_N and R_P, are nonlinearly related to N and P. Therefore, the continuity equations for holes and electrons, (4) and (5), are both nonlinear, and superposition does not apply to the junction space-charge region.

The results of this section are illustrated by the equivalent-network representation of the solar cell in Fig. 4. The dashed lines that connect the current generators representing the quasi-neutral regions are closed or open depending on whether superposition is applicable or not in the quasi-neutral regions. The breaks in connection in the space-charge region representation indicate that superposition is never valid in the junction space-charge region.

Although the principle of superposition never applies to the junction space-charge region, the inapplicability does not necessarily invalidate the resolution of the solar-cell current-voltage characteristics indicated in (1). Using Fig. 4, we now consider special cases that illustrate this.

2.1 Cases for which Eq. (1) applies

Case A: Here the quasi-neutral regions dominate in determining both the photocurrent and the dark current. Low injection prevails throughout the quasi-neutral emitter and base, and series resistance is negligible. Thus the dashed lines in Fig. 4 are short circuits, indicating that superposition applies. From Fig. 4,

$$J = (J^{O}_{QNB} + J^{O}_{QNE}) - (J^{D}_{QNB} + J^{D}_{QNE})$$

$$\triangleq J^{O}_{QNR} - J^{D}_{QNO}[\exp(qV/kT) - 1] \qquad (17)$$

which is consistent with (1).

Case B: Here the conditions are those stated for case A except that the space-charge region now also contributes significantly to the photocurrent. From Fig. 4,

$$J = \left(J^{O}_{QNR} + J^{O}_{SCR}\right) - J^{D}_{QNO}[\exp(qV/kT) - 1] \qquad (18)$$

Case C: Here the dark current of the cell is dominated by the space-charge region and the photocurrent is dominated by the quasi-neutral regions. Series resistance is negligible. Thus, from Fig. 4 and the theory of dark p-n junction diodes [6], we have

$$J = J^{O}_{QNR} - J^{D}_{SCO}[\exp(qV/m_{sc}kT) - 1] \qquad (19)$$

Case D: Here the conditions are those stated in case A except that the space-charge and quasi-neutral regions both contribute significantly to the dark current. Thus, from Fig. 4 and ref. (6),

$$J = J^{O}_{QNR} - \left(J^{D}_{QNO}[\exp(qV/kT)-1] + J^{D}_{SCO}[\exp(qV/m_{sc}kT)-1]\right), \qquad (20)$$

again in agreement with (1).

Discussion: For cases A, B, and C, the open-circuit voltage has the simple form,

$$V_{OC} = \frac{mkT}{q} \ln\left[\frac{J^{O}}{J_{DO}}\right], \qquad (21)$$

where $m = 1$ for cases A and B, and $m = m_{sc}$ for cases C. The open-circuit voltage for case D is the solution for V of (20) when $J = 0$, but no simple explicit expression for V_{OC} exists.

The cases just described have practical importance. For example, cases A and B can describe a p-n-junction solar cell made

on a single-crystal silicon base having light or moderate doping concentration. Cases C and D can describe cells having highly-doped base regions. For such cells, the emitter region can contribute significantly to the dark current [7].

To demonstrate the validity of (19) and (20) for cases C and D, we measured the illuminated and dark I-V characteristics of an n-on-p silicon solar cell having a highly-doped base region ($N_{AA} = 10^{17}$ cm^{-3}). For this cell the thinness of the space-charge region causes the generation in the quasi-neutral base to dominate in determin the photocurrent. At voltages V near V_{OC} for one-sun illumination, the space-charge and quasi-neutral regions both contribute to the dark current (case D). For the current range resulting from an illumination level of 1/100 sun, however, the recombination in the space-charge region alone determines the dark current (case C). Our measured data showed excellent agreement with (1) for both levels of illumination.

Further experimental evidence of the validity of (1) for the low-resistivity silicon cells of interest in this report appears in Chapter IV where we found that the value for the current I_{QNO} determined by dark I-V measurements agreed well with that determined by illuminated I-V measurements.

2.2 Cases for which Eq. (1) does not apply

Any of the following conditions will invalidate the principle of superposition and thus (1):

(a) the space-charge region contributes importantly to both the photocurrent and the dark current; or

(b) the carrier concentrations in the quasi-neutral regions exceed low-injection levels; or

(c) the series resistance contributes significantly to the cell current-voltage characteristics; or

(d) the material parameters, such as the minority-carrier lifetime, depend on the illumination level; or

(e) the volume of the region producing the photocurrent changes appreciably as the cell is loaded (and the terminal voltage V changes).

The invalidity of (1) for CdS cells has been discussed and shown experimentally [8]. The invalidity of (1) for amorphous silicon (a-Si) cells [9] and the consequent poor fill factor probably arises, in part, from the decrease in volume of the junction space-charge region that accompanies loading of the cell. Because the diffusivity and hence the diffusion length of the quasi-neutral regions of a-Si cells is small, the photocarriers generated in the junction space-charge region dominate in determining the photocurrent I. Thus the invalidity of (1) for a-Si cells owes its origin in part to condition (e) listed above and, in part, to condition (a).

Experiments showing the invalidity of (1) for single-crystal silicon cells will be discussed in the following sections, which treat the solar-cell characteristics for cases (b) and (c).

III. HIGH INJECTION IN THE QUASI-NEUTRAL BASE

An important example of high injection occurs in the quasi-neutral base region of a solar cell exposed to concentrated sunlight [10]. Despite the inapplicability of superposition to this cell from a strict standpoint, an analytic description based on superposition can be developed for the case of extreme high-level injection where $P \simeq N$ in the base region. For this case, superposition yields [10]

$$J \simeq J_N(0) = J_N(0)\Big|_{\substack{G^O = 0 \\ \Delta N(0) \neq 0}} + J_N(0)\Big|_{\substack{G^O \neq 0 \\ \Delta N(0) = 0}}$$

$$\triangleq -J_D + J_{UPC} \,. \tag{22}$$

here. In (22), J_D is the dark current-voltage characteristic of the cell. The term J_{UPC} in (22) is the photocurrent in a highly illuminated cell to which a reverse bias is applied to insure $\Delta N(0) = 0$; J_{UPC} is essentially the maximum current that can be drawn from the solar cell for a given level of illumination. We thus call it the uncompensated photocurrent. In general, $J_{UPC} > J_{SC}$.

Using (22) and including effects of high injection in the base region, one can derive analytical expressions for the open-circuit

voltage V_{OC} of highly-illuminated silicon solar cells [10]. In Fig. 5, values of V_{OC} calculated from these expressions for 10Ω-cm n^+-p cells [(V_{OC} proportional to $(2/b+1)(kT/q)\ln(J_{UPC}/J_{DO})$] and 4Ω-cm p^+-n cells [(V_{OC} proportional to $(2b/b+1)(kT/q)\ln(J_{UPC}/J_{DO})$] are plotted against J_{UPC}. These dependencies of V_{OC} on J_{UPC} are compared at several levels of illumination with values of V_{OC} calculated from exact numerical solutions of (2) through (7). These results are contrasted with the classical relation, derived from (1),

$$V_{OC} = (kT/q)\ln(J_{SC}/J_{DO}) \quad , \tag{23}$$

which is a special case of (21). At low-injection levels, $J_{UPC} \simeq J_{SC}$; otherwise, $J_{UPC} > J_{SC}$, because a considerable potential difference can develop across the quasi-neutral base [10]. The inapplicability of (1) is apparent in Fig. 5. This results because the system is not strictly linear [10].

The theoretical results are supported by the experimental data plotted in normalized fashion against the measured J_{UPC} for three types of n^+-p solar cells: a cell having a base resistivity of 10 ohm-cm, one made with a back-surface field (BSF) and the other without a BSF. At high levels of illumination (large J_{UPC}), high injection occurs in the base of the 10 ohm-cm cells at the open-circuit condition. For the 10-ohm-cm cell without a BSF, the measured dependence of V_{OC} on J_{UPC} agrees with the theoretical predictions of Fig. 5 and demonstrates experimentally that (1) is invalid. The V_{OC} dependence observed for the BSF cell again demonstrates the inapplicability of superposition. The nonlinearities associated with high injection in the base region of this cell present an analytical problem different from that describing a non-BSF cell.

Basic corrections of classical theory required by these nonlinearities will be treated in a later publication.

High injection does not occur in the 0.3Ω-cm cell, and its V_{OC} vs. J_{UPC} characteristic agrees with the classical result expressed in (23).

IV. SERIES RESISTANCE

In a p-n-junction solar cell, series resistance R_S can originate in the metal contacts, in the metal-semiconductor interface, in the emitter, and in the base. The presence of R_S invalidates the direct use of superposition. To illustrate this, consider, as the system under study, a p-type quasi-neutral base region. Though the electron continuity equation, (4), remains linear for low injection, the presence of R_S results in a nonlinear boundary condition relating ΔN and J_N:

$$\Delta N(0) \propto [\exp(qV/kT)\exp(qIR_S/kT) - 1] , \tag{24}$$

where I depends on $J_N(0)$. The nonlinearity of (24) precludes the use of superposition in which $\Delta N(0)$, defined by (24), is regarded as an independent excitation.

A solar cell with significant R_S can be treated analytically by separating R_S from the intrinsic system, as in Fig. 7. The intrinsic system is defined so that

$$\Delta N(0) \propto [\exp(qV_{IS}/kT) - 1] . \tag{25}$$

Since $\Delta N(0)$ thus defined depends only on the voltage V_{IS} across the system, it can be regarded as an independent excitation. Thus the intrinsic system of Fig. 7 can be treated as described in Section II, where we indicated the conditions for which superposition applies.

Use of superposition requires that $\Delta N(0)$ be set to zero, which defines the photocurrent J_{UPC}. As for the high-injection condition described in Section III, here also a short circuit applied across the cell terminals fails to make $\Delta N(0)$ because

$$V = V_{IS} - I R_S \tag{26}$$

From (25) we see that $\Delta N(0) = 0$ implies $V_{IS} = 0$, and from (26) that a reverse bias of about $I_{UPC}R_S$ must therefore be applied to the solar cell to experimentally determine J_{UPC}. We note again that $J_{UPC} > J_{SC}$, where $J_{SC} = J(V=0)$.

For low-injection conditions, R_S is a constant, independent of I, and can be determined experimentally [11].

V. DISCUSSION

The basis underlying this Appendix is the superposition principle. Its use here provides insight about the approximation of (1) that the characteristic of an illuminated solar cell is the dark current-voltage characteristic shifted by the short-circuit current. Interpreted from the standpoint of the superposition principle, the current I(V) in (1) is the sum of the response to two excitations applied independently, one at a time. One excitation is the hole-electron optical generation rate resulting from the sunlight. The other is the excess carrier concentration at each edge of the junction space-charge region, which is related to the voltage difference across the cell terminals. The two responses are therefore the short-circuit current and the dark-current characteristic.

The optical generation rate and the excess carrier concentration at the SCR edges are chosen as the excitations because they are the independent variables in the boundary-value problem describing the cell. These variables are linearly related to the current and to the excess carrier concentrations within the cell under certain well-defined conditions which, therefore, are necessary for superposition to apply. These conditions are:

(a) the junction space-charge region may contribute importantly to either the photocurrent or the dark current, but not to both;

(b) the carrier concentrations in the quasi-neutral regions must stay within low-injection levels;

(c) the series resistance must contribute negligibly to the cell current-voltage characteristics;

(d) the material parameters, such as the minority-carrier lifetime, must be essentially independent of the illumination level; and

(e) the volume of the regions that contribute appreciably to the photocurrent must stay essentially constant as the cell is loaded.

We have described corrections to superposition-based theory if conditions (b) or (c) are violated. The violation of condition (b) discussed here relates to an application of much practical importance—the performance of (single-crystal) silicon p-n junction cells in concentrated sunlight. Although in a strict sense the superposition principle is invalid for this application, we used superposition in developing the correction. This use led to a theory that agreed well both with laboratory experimentation and with the exact computer solution of the underlying

differential equations (2) - (7).

This is the first application of the superposition principle of differential-equation theory to the analysis of solar cells. We believe that this principle offers valuable insight about the range of validity of (1) and of the considerable simplifications that (1) yields. Beyond this, the treatment discussed here of a cell in concentrated sunlight has shown that superposition provides a basis from which to develop corrections when (1) fails to hold. We anticipate that the superposition principle will prove useful also in applications other than those discussed in detail here, including applications to cells made of materials other than single-crystal silicon.

REFERENCES FOR APPENDIX

1. P. W. Berg and J. L. McGregor, Elementary Partial Differential Equations, p. 7, Holden-Day, San Francisco, 1963.

   G. A. Korn and T. M. Korn, Mathematical Handbook for Scientists and Engineers, Sections 9.3-1, 10.4-1, 10.4-2, and 15.4-2, McGraw-Hill, 1961.

2. D.F. Tuttle, Network Synthesis, p. 19, John Wiley & Sons, 1958.

   H. H. Skilling, Electrical Engineering Circuits, p. 353, John Wiley & Sons, 1965.

3. J. L. Bower and P. M. Schultheiss, Introduction to the Design of Servomechanisms, pp. 11, 100, John Wiley & Sons, 1958.

4. W. Shockley, "The Theory of p-n Junctions in Semiconductors and p-n Junction Transistors," Bell Sys. Tech. J., Vol. 28, pp. 435-489, July 1949.

5. F. A. Lindholm and C. T. Sah, "Fundamental Electronic Mechanisms Limiting the Performance of Solar Cells," IEEE Trans. Electron Devices, April 1977.

6. C. T. Sah, R. N. Noyce, and W. Shockley, "Carrier Generation and Recombination in p-n Junctions and p-n Junction Characteristics," Proc. IRE, Vol. 45, pp. 1228-1243, Sept. 1957.

   C. T. Sah, "Effect of Surface Recombination and Channel on p-n Junction and Transistor Characteristics," IRE Trans. on Electron Devices, Vol. ED-9, pp. 94-108, Jan. 1962.

7. F. A. Lindholm, A. Neugroschel, C.T. Sah, M. P. Godlewski, and H. W. Brandhorst, Jr., "Methodology for the Experimental Detemination of Gap Shrinkage and Lifetimes in the Emitter and Base of Solar Cells and other p-n Junction Devices," IEEE Trans. Electron Devices, April 1977; also Record of Twelfth Photovoltaic Specialists Conf., Nov. 1976.

8. K. W. Böer, "CdS/Cu_2S Heterojunction Model," Proc. Sharing the Sun, Int. Conf., Photovoltaics, Vol. 7, pp. 130-145, Winnipeg, Manitoba, Canada, Aug. 1976.

9. C. R. Wronski, D. E. Carlson, R. E. Daniel and R. R. Triano, "Electrical Properties of a-Si Solar Cells," Technical Digest 1976 Int. Electron Devices Meeting (76CH1151-OED), pp. 75-78, Dec. 1976; also D.E. Carlson and C.R. Wronski, Appl. Phys. Lett., vol. 28, No. 11, P. 602 (1976).

10. J. G. Fossum and F. A. Lindholm, "The Dependence of Open-Circuit Voltage on Illumination Level in p-n Junction Solar Cells," IEEE Trans. Electron Devices, April 1977.

11. M. Wolf and H. Rauschenbach, "Series Resistance Effects on Solar Cell Measurements," Advanced Energy Conversion, Vol. 3, pp. 455-479, Apr.-June, 1963.

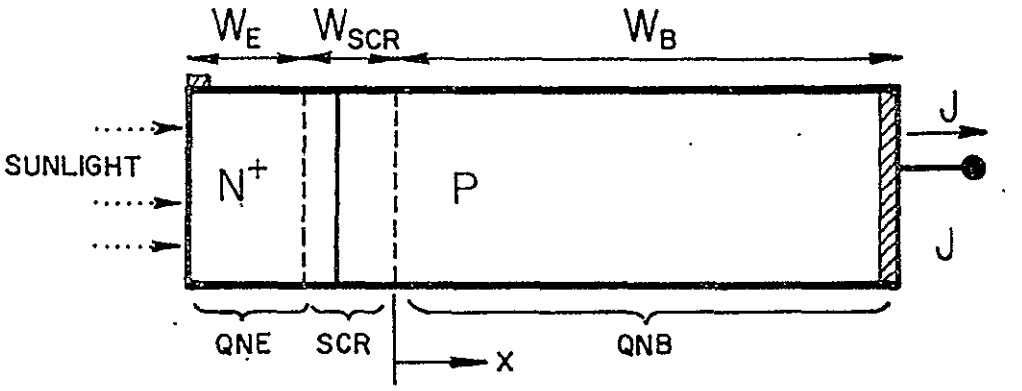

Fig. 1 One-dimensional model of a p-n-junction solar cell.

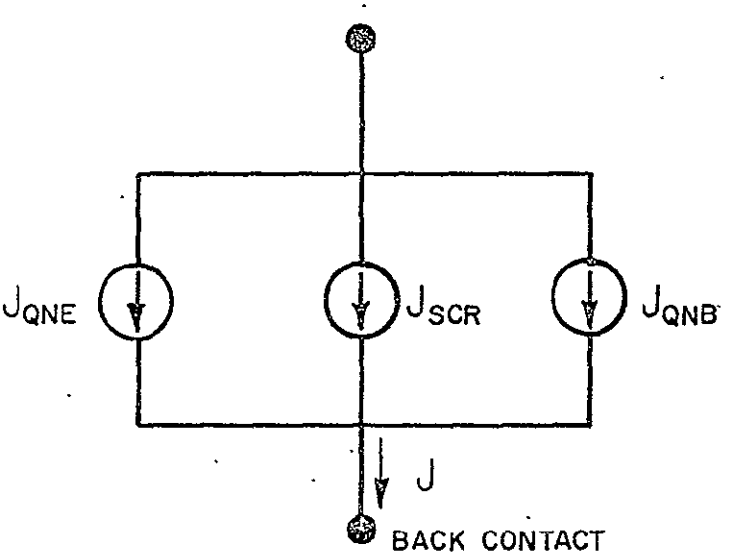

Fig. 2 The Kirchhoff current law holds regardless of the applicability of superposition.

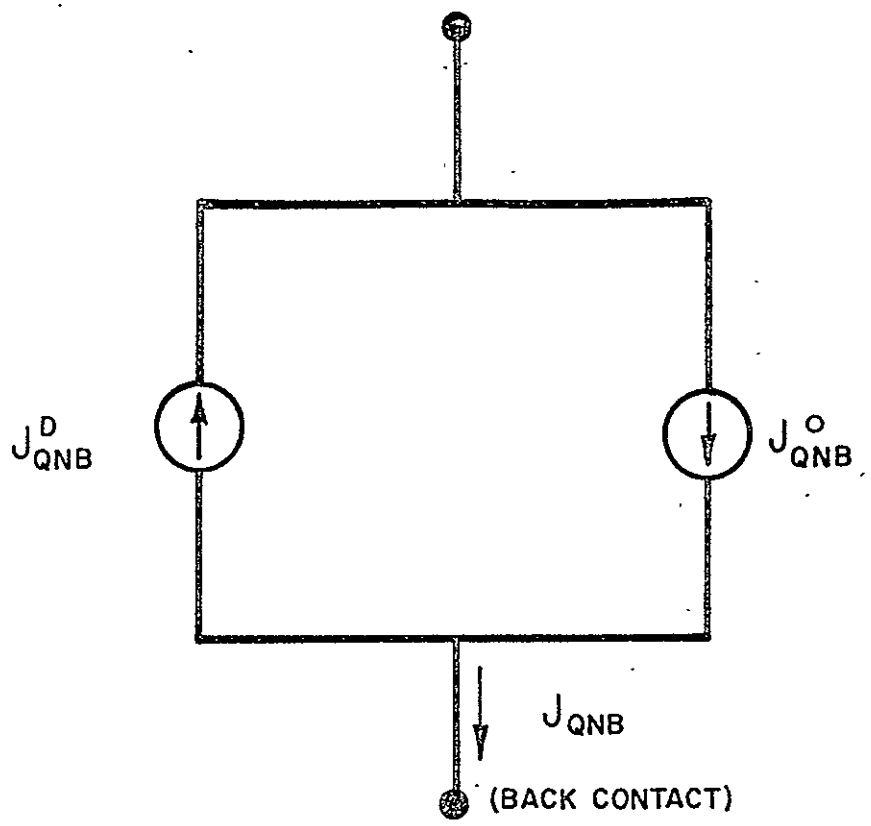

Fig. 3 Equivalent circuit for the quasi-neutral base if superposition applies. A similar equivalent circuit represents the quasi-neutral emitter.

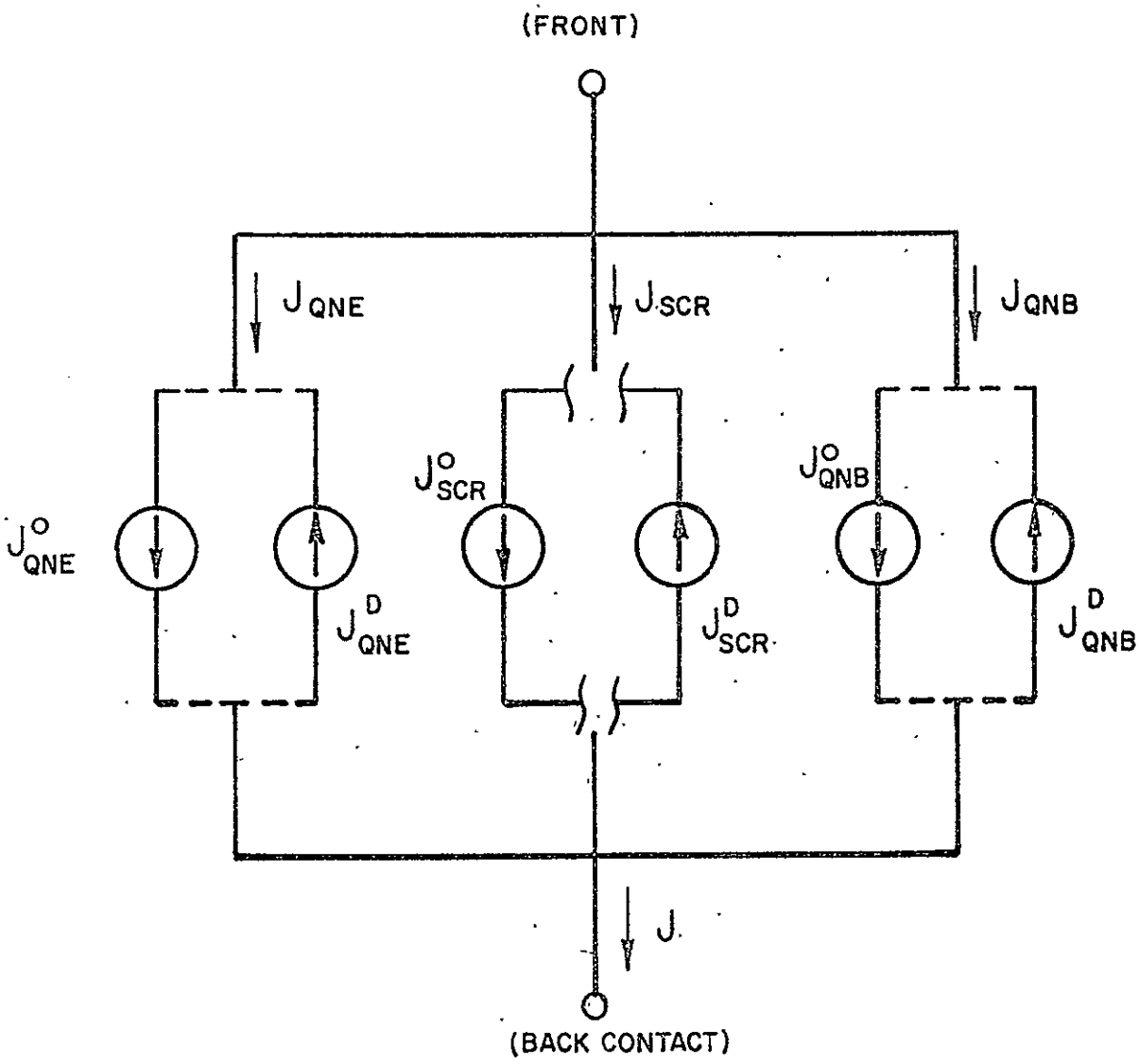

Fig. 4. Equivalent circuit for the entire solar cell.

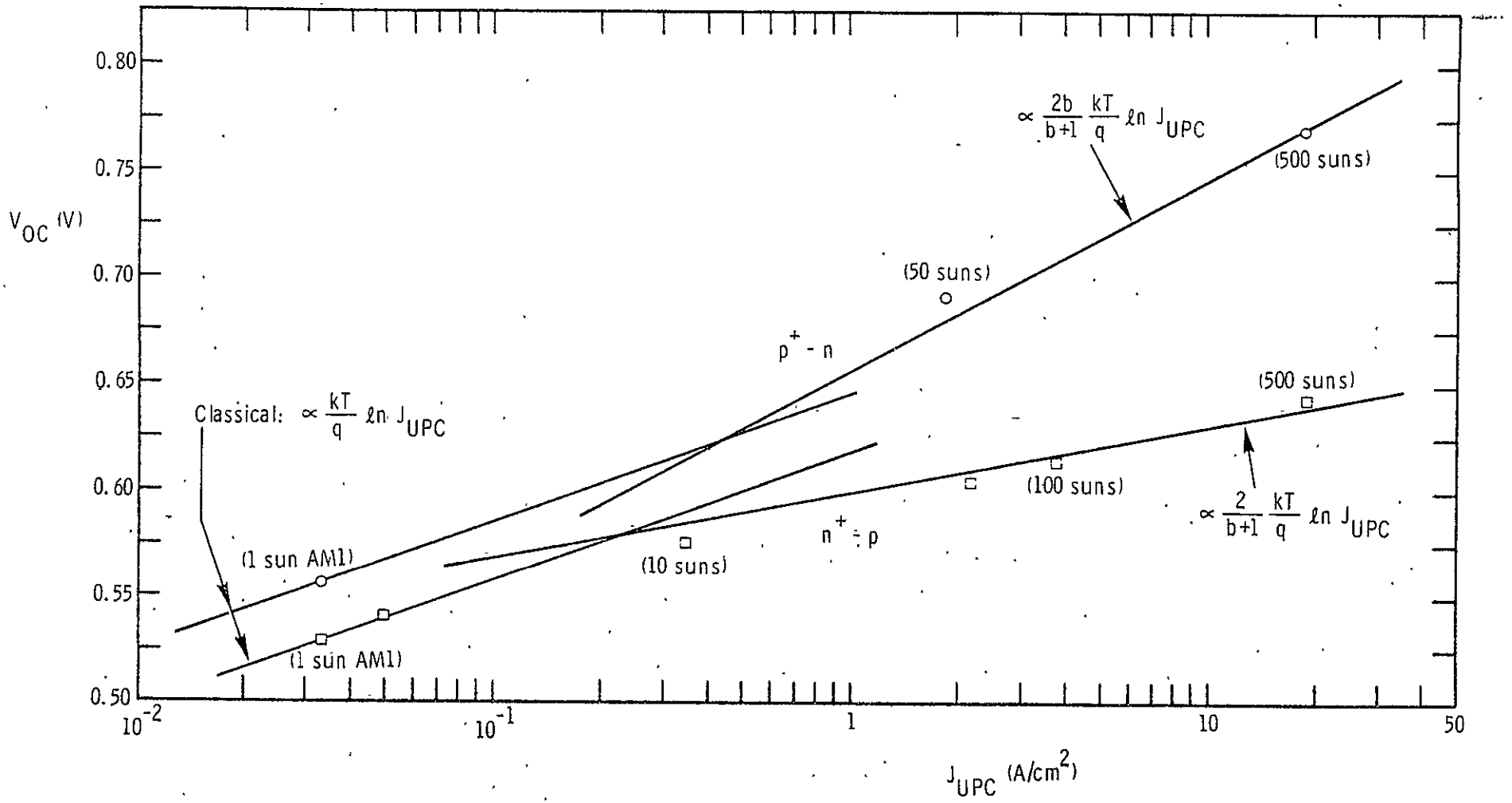

Fig. 5 Superposition-based theoretical dependence of V_{OC} showing invalidity of Eq. (1) for high injection but showing agreement with values obtained from computer solution of the differential equations.

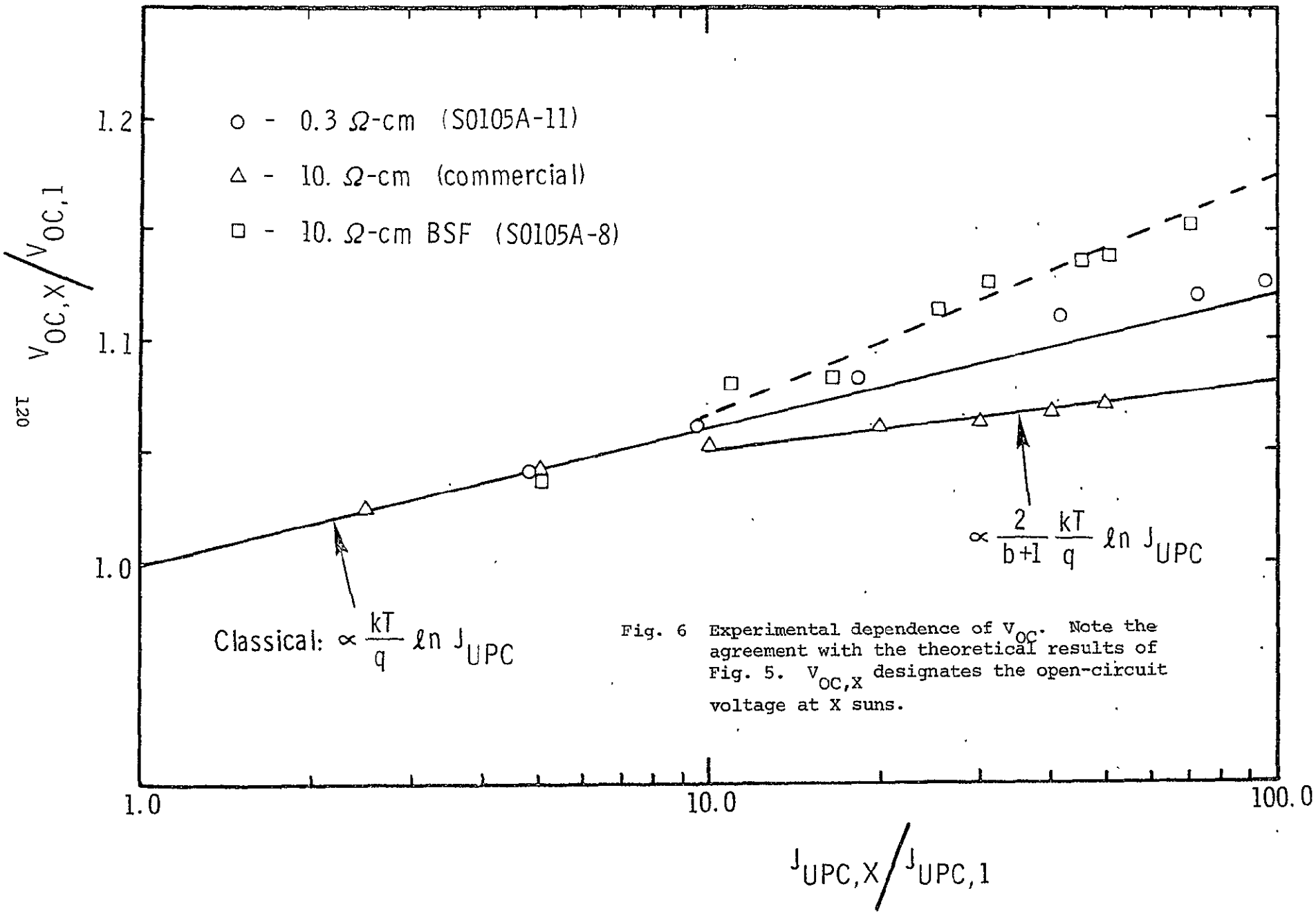

Fig. 6 Experimental dependence of V_{OC}. Note the agreement with the theoretical results of Fig. 5. $V_{OC,X}$ designates the open-circuit voltage at X suns.

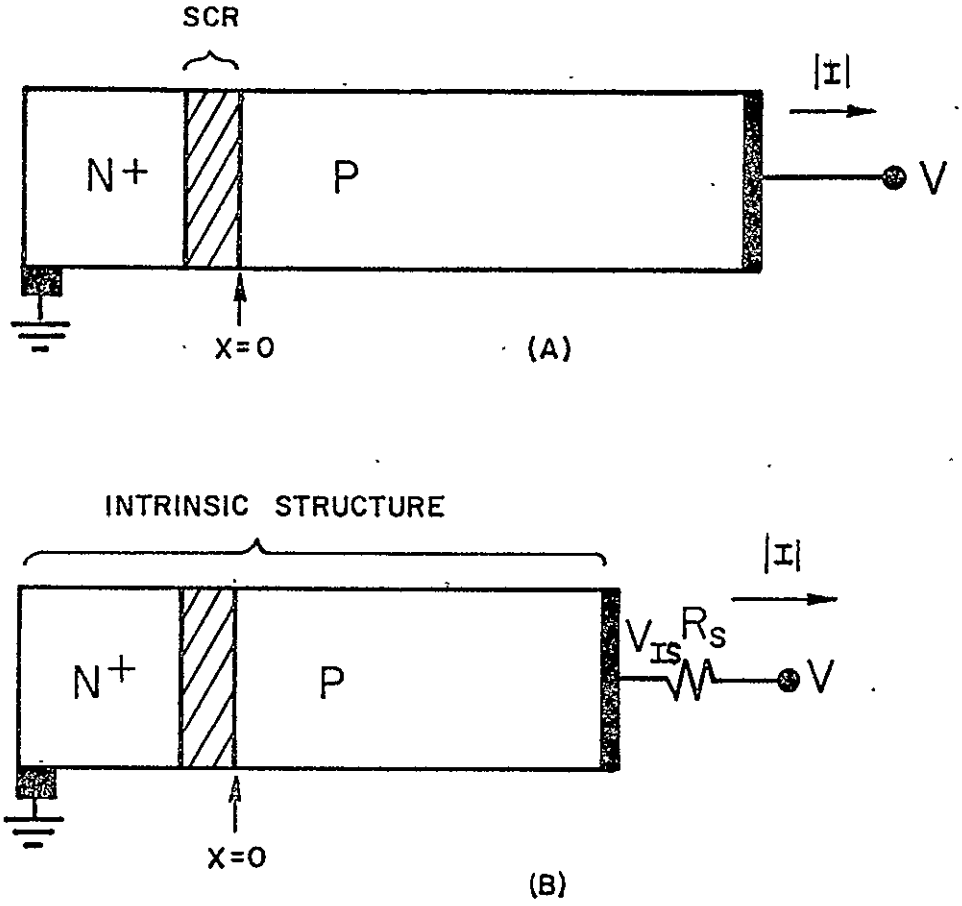

Fig. 7 (a) Entire solar cell in which $\Delta N(0)$ depends nonlinearly on I;

(b) Intrinsic solar cell in which $\Delta N(0)$ is proportional to $[\exp(qV_{IS}/kT) - 1]$.